5-2005

Investigating Keratoconus Using Optical Eye Modeling

Kevin Charles Baker
University of Tennessee - Knoxville

To the Graduate Council:

I am submitting herewith a thesis written by Kevin Charles Baker entitled "Investigating Keratoconus Using Optical Eye Modeling." I have examined the final electronic copy of this thesis for form and content and recommend that it be accepted in partial fulfillment of the requirements for the degree of Master of Science, with a major in Physics.

Ying-Ling Chen, Major Professor

We have read this thesis and recommend its acceptance:

James W. L. Lewis, Horace W. Crater

Accepted for the Council:
Carolyn R. Hodges

Vice Provost and Dean of the Graduate School

(Original signatures are on file with official student records.)

To the Graduate Council:

I am submitting herewith a thesis written by Kevin Charles Baker entitled "Investigating Keratoconus Using Optical Eye Modeling." I have examined the final electronic copy of this thesis for form and content and recommend that it be accepted in partial fulfillment of the requirements for the degree of Master of Science, with a major in Physics.

Ying-Ling Chen
Major Professor

We have read this thesis
and recommend its acceptance:

James W. L. Lewis

Horace W. Crater

Accepted for the Council:

Anne Mayhew
Vice Chancellor and
Dean of Graduate Studies

(Original signatures are on file with official student records.)

Investigating Keratoconus Using Optical Eye Modeling

A Thesis

Presented for the

Master of Science Degree

The University of Tennessee, Knoxville

Kevin Charles Baker

May 2005

Acknowledgments

I would like to take this opportunity to thank all those who made this thesis possible. I would like to thank my thesis advisor Dr. Ying-Ling Chen for her numerous hours spent assisting me in the completion of this thesis. I would also like to thank my other committee members Dr. James W. L. Lewis and Dr. Horace W. Crater for their many suggestions/corrections to this thesis. Finally, I would like to thank my wife Jeni, without her support I wouldn't have made it this far.

Abstract

Keratoconus (KC) is a corneal atrophy which causes a conical extrusion (cone). It is often misdiagnosed as optical defocus with astigmatism. In this thesis, computer KC eye models for various conditions are constructed. Using the KC eye model the influence on visual performance including the consequent refractive errors and the higher-order aberrations of KC eyes was investigated. The affects of cone shape, dimension (volume), and location on visual performance are also discussed. The modeled KC eyes are additionally used to evaluate the performance of a common eye vision-screening instrument. The simple photorefraction (PR) technique uses only one small light source with a camera to photograph ocular reflection patterns. Computer optical ray tracing was performed to simulate the PR images of both KC eyes and astigmatic eyes. The simulation results shown indicate the ability to detect and differentiate KC from normal refractive errors.

Contents

1 Introduction to Keratoconus **1**

1.1 Keratoconus Overview 1

1.2 Diagnosing KC 4

1.3 Classification 7

1.4 Objectives 9

2 Keratoconus Eye Model **10**

2.1 Topography of Cornea 11

2.2 Zernike Polynomials 12

2.3 Eye Models 19

2.4 Keratoconus Cornea Model 21

3 Keratoconus Eye Visual Performance **25**

3.1 Evaluating Visual Performance Through Wave Front Aberration 26

3.2 KC Eye Visual Performance Analysis 31

3.3 Cone Location Visual Affects 42

3.4 Cone Dimension Visual Affects 48

3.5 Cone Shape Visual Affects 50

4 Keratoconus Analysis Using Photorefraction **54**

4.1 Photorefraction Description 55

4.2 Photorefraction Images of Keratoconus and Astigmatism of Same Equivalent Prescription 57

5 Summary **64**

Bibliography **67**

Vita **72**

List of Tables

1.1 Classification of Keratoconus Based on Dioptric Power of Cornea. [3]. . 7

1.2 Classification of Keratoconus Based on Size of Cone. [4]. 8

2.1 Geometry of the Schematic Wide-Angle Eye Model[16]. 20

3.1 Keratoconus Cone Parameters. 36

3.2 14 Keratoconus on Axis: Equivalent Prescription. 38

3.3 14 Keratoconus Average Location: Equivalent Prescription. 39

3.4 14 Keratoconus Far Location: Equivalent Prescription. 39

4.1 Photorefraction Parameter Affects. 57

List of Figures

1.1 Profile View of Keratoconus[3]. 2

1.2 Normal vs. Keratoconus Cornea. 2

1.3 Image of Scissor's Reflex in Keratoconus Patient [3]. 5

1.4 EyeSys Photokeratoscope With Placido Disk 6

1.5 Drawing illustrating round (nipple) left, and oval (sagging) right [4]. . . 8

2.1 Z_0^0: Describes surface mean height. 14

2.2 Z_1^1: Describes surface tilt, Z_1^{-1} is a 90° rotation of Z_1^1. 14

2.3 Z_2^0: Describes the average curvature of the surface. 15

2.4 Z_2^2: Describes surface astigmatism, Z_2^{-2} is a 45° rotation of Z_2^2. 15

2.5 Z_3^1: Describes an irregularity structure in surface, Z_3^{-1} is a 90° rotation of Z_3^1. 16

2.6 Z_4^0: Describes an additional term for the curvature of the surface, also spherical aberration. 16

2.7 Model Eye Used in Ray-Tracing Code. 21

2.8 Typical 3-Dimensional View of Modeled Keratoconus Cone. 24

2.9 Typical 2-Dimensional View of Modeled Keratoconus Cone. 24

3.1 Eye's Wave Front Aberration. 28

3.2 Measured Cone Height Distribution [22]. 33

3.3 Measured Cone Dimension Distribution. The red cross shows the mean value and standard deviations.[22]. 34

3.4 Measured Cone Volume Distribution [22]. 35

3.5 Measured Cone Location Distribution, T and N indicate the temporal and nasal directions. The red symbols and crosses in the 2 plots indicate the mean locations and standard deviations of the distributions. [22]. . . 36

3.6 14 Synthetic KC Cones Describing 4 Degrees (mild, moderate, advanced, and severe). The lower portion illustrates three cone locations on the cornea used during the calculations. 37

3.7 Keratoconus Normal Refractive Errors For 14 Different Cones at 3 Different Locations. 41

3.8 Keratoconus Cone Location Visual Prescription Affects. Top: Spherical Equivalent Power. Middle: Absolute Cylindrical Power. Bottom: Root-mean-square of higher-order aberrations $W_{3,4}$. 43

3.9 Surface Curvature For Small Cone ($\sigma_x/\sigma_y/h_0$). 45

3.10 Surface Curvature For Medium Cone ($\sigma_x/\sigma_y/h_0$). 46

3.11 Surface Curvature For Large Cone ($\sigma_x/\sigma_y/h_0$). 47

3.12 Keratoconus Cone Dimension Visual Prescription Affects. Top: Spherical Equivalent Power. Middle: Absolute Cylindrical Power. Bottom: Root-mean-square of higher-order aberrations $W_{3,4}$. 49

3.13 Keratoconus Cone Shape Visual Prescription Affects. Top: Spherical Equivalent Power. Middle: Absolute Cylindrical Power. Bottom: Root-mean-square of higher-order aberrations $W_{3,4}$. 52

4.1 Eccentric Photorefraction For Farsighted, Normal, Nearsighted Eye. . . 56

4.2 Keratoconus Coaxial Photorefraction Images In Three Different Locations. Left column corresponds to cones on visual axis, middle column to average cone location, and right column to outlying cone location. The four numbers correspond to Spherical (D), Cylindrical (D),Astigmatism Axis, $W_{3,4}$ (μm). 58

4.3 Keratoconus Eccentric Photorefraction Pupil Image For Cones Located On Visual Axis. Left column corresponds to KC eyes, while right column corresponds to Equivalent Astigmatic Eyes. The four numbers correspond to Spherical (D), Cylindrical (D), Astigmatism Axis, $W_{3,4}$ (μm). 60

4.4 Keratoconus Eccentric Photorefraction Pupil Image For Cones Located At Average Position. Left column corresponds to KC eyes, while right column corresponds to Equivalent Astigmatic Eyes. The four numbers correspond to Spherical (D), Cylindrical (D), Astigmatism Axis, $W_{3,4}$ (μm). 61

4.5 Keratoconus Eccentric Photorefraction Pupil Image For Cones Located At Outlying Position. Left column corresponds to KC eyes, while right column corresponds to Equivalent Astigmatic Eyes. The four numbers correspond to Spherical (D), Cylindrical (D), Astigmatism Axis, $W_{3,4}$ (μm). 62

Chapter 1

Introduction to Keratoconus

1.1 Keratoconus Overview

Keratoconus (KC) is an eye condition in which there is a noninflammatory thinning of the cornea. Due to the intraocular pressure of the eye, the thinning cornea bulges to form a conical shape (Fig. 1.1). Figure 1.2, illustrates the surface of a normal and a KC cornea. The epithelium is a cellular avascular layer on the outside of the cornea, the endothelium is cellular layer on the inside of the cornea. The stroma is the middle layer of the cornea which comprises about 90 % of the cornea. The abnormal curvature caused by KC changes the eye's refractive power and produces myopic and astigmatic power symptoms.

Refractive power is the inverse of focal length which is usually measured in inverse meters or diopters (D). Myopia (nearsightedness) is a spherical refractive error in which the light rays entering the eye focus in front of the retina. This is caused when the eye's

Figure 1.1: Profile View of Keratoconus[3].

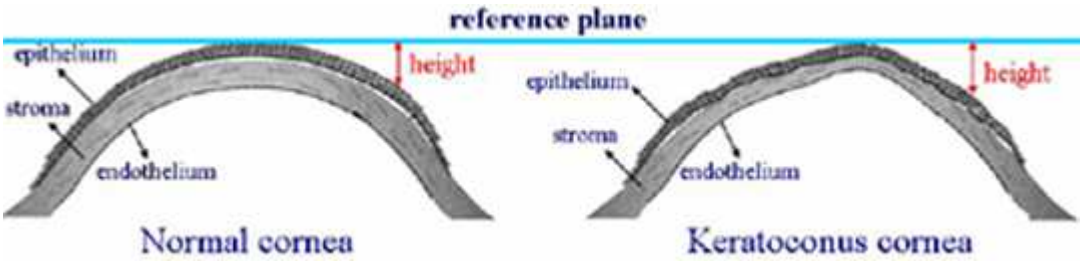

Figure 1.2: Normal vs. Keratoconus Cornea.

optical power is too strong or when the eye's axial length is too long. Astigmatism, a cylindrical refractive error, occurs when the ocular rotational-symmetry vanishes and the toricity, two optical powers at right angles, of the refractive surfaces causes the optical system to have two focal planes [2]. These two types of refractive errors can be easily corrected using spectacles or contact lenses. Since KC is progressive and has an irregular power distribution, it can be difficult to correct.

In the early stages KC may be corrected by spectacles [1]. As KC progresses, the irregular astigmatism increases and cannot easily be corrected by spectacles, and rigid contact lenses are required to correct KC [1, 3]. Rigid contact lenses can improve the vision more effectively by depressing the cone down, however, a problem can arise if the contact lens rubs the corneal surface which can further weaken the cornea or introduce corneal scarring. Approximately 20% of keratoconus patients eventually require a cornea transplant [3].

It is difficult to determine the frequency of KC. Some estimates are that one in every two thousand people in the United States have keratoconus [3]. However, this number may be too small because it is believed that a large number of people with KC are misdiagnosed. Keratoconus usually develops in the teenage years and seldom progress after thirty years of age [3]. It shows no preference in gender, and in most cases it is bilateral [3, 5].

There are many different ideas on how keratoconus is caused, but one idea is a change in the biochemical and physical corneal tissue [3]. There are also indications

that it is hereditary [1, 3]. Wearing rigid contact lenes for a long time has also been found to induce keratoconus [1, 3].

1.2 Diagnosing KC

Recognizing keratoconus can be difficult because of its appearance of myopia and astigmatism. KC is often misdiagnosed in the early stages as myopia (nearsightedness) with astigmatism. Some indications of KC include frequent eye prescription changes or eye pain if contact lenses are worn [3]. Some of the different diagnosis aids for keratoconus include: retinoscopy, slit lamp examination, and photokeratoscope or topographer placido disc.

Retinoscopy can also be used as an aid to detect KC [5]. Retinoscopy is a method of examining the pupil's light reflex to determine the eye's refractive error. Retinoscopy indicates advanced cases of keratoconus as a scissors reflex, or direct ophthalmoscopy shows a shadow, (Fig. 1.3) [1, 3, 5].

A slit lamp examination is also a useful aid to detect keratoconus. A slit lamp is a microscope that uses a slit beam of light to magnify the cross section of the cornea. With the slit lamps aid it is possible to view many advanced indicators of keratoconus. These include: Fleischer's ring, stress lines of Vogt, corneal thinning and scarring, various types of staining with and without lens wear, and increased visibility of corneal nerves [1, 3]. A Fleischer ring is a yellow-brown to olive-green ring of pigment which may or may not completely surround the base of the cone. Lines of Vogt are small and brushlike

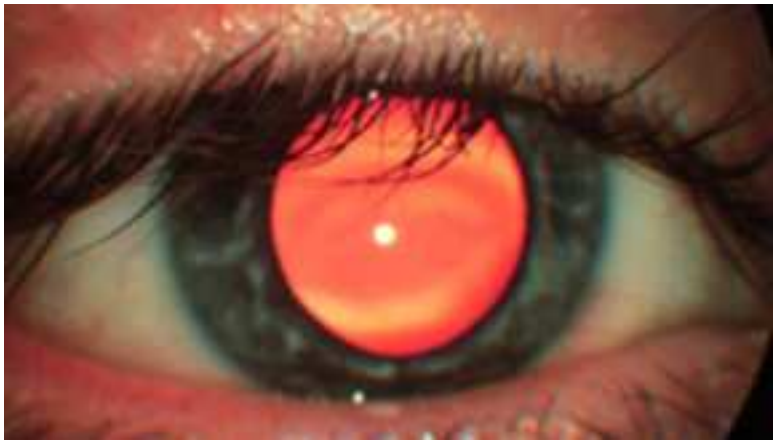

Figure 1.3: Image of Scissor's Reflex in Keratoconus Patient [3].

lines.

The keratometer is another diagnosing aid used to measure the curvature of the corneal surface. It is a beneficial instrument used to determine the astigmatism. Instead of measuring the whole corneal curvature, the keratometer detects the steepest and flattest curvatures. This gives an indication to the topography of the corneal surface.

The photokeratoscope, (Fig 1.4) is a new diagnosing aid that measures the topography of the cornea. The photokeratoscope takes a reflection image of the placido disk off the cornea [6]. The computer analyzes the shape of the placido disk, circular shaped mires, to create the cornea's two-dimensional topographical map. Using computer-assisted analysis, plots of the cornea raw height or the refractive power can be obtained. One can also obtain a simulated keratometry (Sim K) value for each cornea [6]. The Sim K value has a high correspondence to the typical keratometry measurement [6].

In addition to the typical dioptric plots, it is also noted that height maps are useful

Figure 1.4: EyeSys Photokeratoscope With Placido Disk

to diagnose KC [7]. Since the height of the cone itself is much smaller than the cornea, it is difficult to locate a KC cone. Therefore, the background cornea must be eliminated to reveal the resultant cone [7]. One technique is to first decompose the corneal surface height into orthogonal functions, and then subtract off the irrelevant terms. Several different orthogonal functions have been studied, but by far the most popular are the Zernike polynomials [7]. Zernike polynomials have been extensively used to analyze the ocular waver front aberration [8, 9].

Zernike polynomials have several advantages over other methods to describe an optical surface. One obvious advantage is that Zernike polynomials are orthonormal over the unit circle. Each Zernike polynomial also represents a physical corneal shape. For example, the Z_2^0 polynomial represents the average corneal curvature, and Z_2^{+2} and Z_2^{-2} describe corneal astigmatism. Zernike polynomials will be discussed in more detail

during section 2.2.

1.3 Classification

There is currently not a standard way of classifying keratoconus. Some prevalent classification criteria include: cone shape, central keratometic reading, or how it progresses [3]. The simplest ways of classifying the degree of keratoconus is using the keratometic reading or the cone shape.

According to the Center for Keratoconus [3], there are four different degrees of keratoconus using the optical power of the cornea. Table 1.1 shows the classification criteria for various degrees of KC based on the dioptric power of the cornea. A normal cornea has an optical power of about forty-three diopters (D), and that of the whole eye is about sixty D. The optical power is the inverted focal length, and the diopter is a measure of optical power in units of inverse meters. The larger dioptric power results in a more severe KC eye, because the light rays will focus farther in front of the retina.

The other common classification system is to use the shape of the cone. Table 1.2, shows three different cone shapes that describe KC. Perry suggested classifying keratoconus as just round and oval cones [4]. Figure 1.5, demonstrates the round and

Table 1.1: Classification of Keratoconus Based on Dioptric Power of Cornea. [3].

Classification	Parameter
Mild	$<$ 45 D in both meridians
Moderate	45-52 D in both meridians
Advanced	52-62 D in both meridians
Severe	$>$ 62 D in both meridians

Table 1.2: Classification of Keratoconus Based on Size of Cone. [4].

Classification	Parameter	Comments
Nipple	small diameter	round shape (5mm)
Oval	large diameter	displaced inferiorly; (> 5mm)
Globus	largest diameter	75% of cornea affected; (> 6mm)

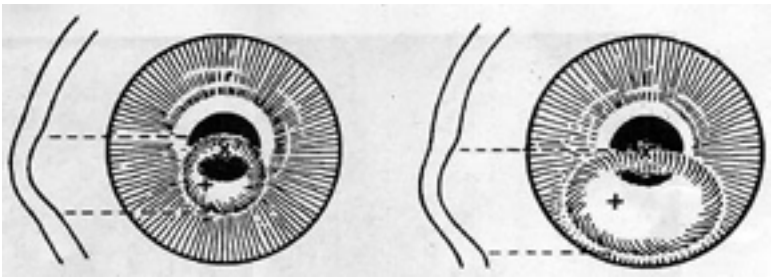

Figure 1.5: Drawing illustrating round (nipple) left, and oval (sagging) right [4].

oval type cones in keratoconus.

There are several different characteristics of the round and oval cones. The round cone is the most common shape. The cone's center usually lies within a few millimeters of the visual axis in the lower nasal quadrant. The oval cone is typically larger and usually lies in the lower temporal quadrant. The oval cone commonly lies farther away from the visual axis, but has a greater dioptric value [4].

The problem with these two classifications is that they are ill-defined. To monitor KC progression a better description needs to be developed. With the advent of the photokeratoscope it is possible to obtain a more quantitative description of the cone's shape and distance from the visual axis. The two different classifications are not independent. Currently, their has been little said on how the shape and location of the cone

will affect the optical power.

1.4 Objectives

A major objective in this investigation is to construct a KC eye model describing various degrees of KC. This KC eye model can be used in future research. The mathematical construction of the KC eye model will be explained in Chapter 2. Various degrees, from mild to severe, of KC eyes are established based on measured KC cone statistical distributions. The optical affects for each cone parameter describing KC, (dimension, shape, and location), are investigated in Chapter 3. Chapter 4 applies the KC eye model to validate a vision screening instrument, based on coaxial and eccentric photorefraction (PR), to differentially diagnose KC from spherical refractive errors.

Chapter 2

Keratoconus Eye Model

Optical modeling of KC eyes can determine how the KC cone affects the eye's visual performance. A medical instruments sensitivity to detect and differential diagnose KC can also be studied before testing on human subjects. Therefore a KC eye model would be quite beneficial. To construct a KC eye model a normal eye's front corneal surface will be modified according to the KC corneal structure. The corneal surface can be established by measuring KC patient cornea topographs. The topography of a KC cornea has been evaluated previously [6, 7, 20, 21, 22, 23]. Typical cone sizes from these papers can be adopted to create a systematic model describing a KC cornea.

Section 2.1 will discuss how the topography of a KC cornea can be determined. A way to view the resulting cone using Zernike polynomials is discussed in section 2.2. Throughout Section 2.3 the details of the normal eye model will be expatiated. The KC eye model is constructed by modifying the normal eye model's corneal surface and

is discussed in Section 2.4.

2.1 Topography of Cornea

The KC cornea surface topography must be obtained and defined before the KC eye model is constructed. There are two different ways to obtain the height map: extracted from dioptric correction data files, or by directly obtaining the elevation file from the photokeratoscope. Appelgate studied the accuracy of both of these methods on different surface types representing the cornea [24]. In Appelgate's study, he obtained the surface topography from calibrated spherical, elliptical, and bicurve surfaces. The surface topography's accuracy was quantified by evaluating the root-mean-squared (RMSE) of the 6400 measured height data points from the known surface elevation.

Appelgate concluded that the extracted method yields surface elevations with an uncertainty of less then 5 μm for spherical and elliptical surfaces. The back calculated technique represented the known surface topography better for spherical and elliptical surfaces, but for abrupt transitions the instrument's elevation files had a better surface fit. [24].

Schwiegerling [7] also evaluated the performance of a video-keratoscope to obtain a cornea surface topography. In his investigation several toric surfaces were studied. A toric surface is one in which two perpendicular meridians are curved in different magnitudes. For the toric surface with the largest curvature difference, 7 D toric (Radius 7.80 x 6.71 mm), the RMSE was determined to be 4.2 μm.

These two investigations show the cornea surface topography can be accurately determined. The RMSE was typically a few microns for a surface representing a cornea. However, KC patients have cone peak heights ranging from 5 to 55 μm [22]. Since the cone heights are greater than the instrument error, the topography can reproduce the KC cone structure and location on the cornea.

2.2 Zernike Polynomials

Due to the magnitude of their characteristic sizes, the KC cone cannot be directly observed in the topography height map of an abnormal cornea. Therefore, a method is required to eliminate the base cornea height to observe the KC cone. One method is to decompose the height map into optically meaningful terms that are based on their refractive contributions. The terms that contain cone information can then be separated and examined. The Zernike polynomials are an obvious choice, because each term has a physical interpretation and they are orthogonal over the unit circle. Zernike polynomials are used as a convenient representation of the ocular wave-front aberration function [8, 25]. More recently, Zernike polynomials have been used to determine the resulting cone structure from video-keratoscope surface data [7, 21, 22, 23]. The Zernike polynomials have been derived and analyzed thoroughly elsewhere [8, 25]. Therefore, only some of the useful properties for this discussion will be discussed here.

Zernike polynomials are defined mathematically as:

$$\begin{aligned} Z_n^{+m}(\rho,\theta) &= \sqrt{2(n+1)}R_n^m(\rho)\cos(m\theta) \\ Z_n^{-m}(\rho,\theta) &= \sqrt{2(n+1)}R_n^m(\rho)\sin(m\theta) \\ Z_n^{m=0}(\rho,\theta) &= \sqrt{2(n+1)}R_n^m(\rho) \end{aligned} \tag{2.1}$$

where

$$R_n^m(\rho) = \sum_{s=0}^{\frac{n-m}{2}} \frac{(-1)^s(n-s)!}{s![\frac{n+m}{2}-s]![\frac{n-m}{2}-s]!}(\rho^{n-2s}) \tag{2.2}$$

n is the order of the polynomial in the radial direction, ρ is the normalized radial coordinate $\frac{r}{r_{max}}$ of the pupil, θ is the normal polar angle, and m is the frequency in the azimuthal direction. The Zernike polynomials are made orthonormal

$$\int\int \rho d\rho d\theta W(\rho) Z_n^m Z_{n'}^{m'} = \delta_{nn'}\delta_{mm'} \tag{2.3}$$

with the appropriate weighting function.

$$\begin{aligned} W(\mathbf{r}) &= \frac{1}{\pi} \qquad \text{for } |\mathbf{r}| \le 1 \\ &= 0 \qquad \text{for } |\mathbf{r}| > 1 \end{aligned} \tag{2.4}$$

The lower order Zernike polynomials represent familiar characteristic shapes as shown in Figs. 2.1-2.6. Z_0^0 represents the surface mean height, Z_1^1 and Z_1^{-1} determine the surface tilt, Z_0^2 describes the surface average curvature, while Z_2^2 and Z_2^{-2}

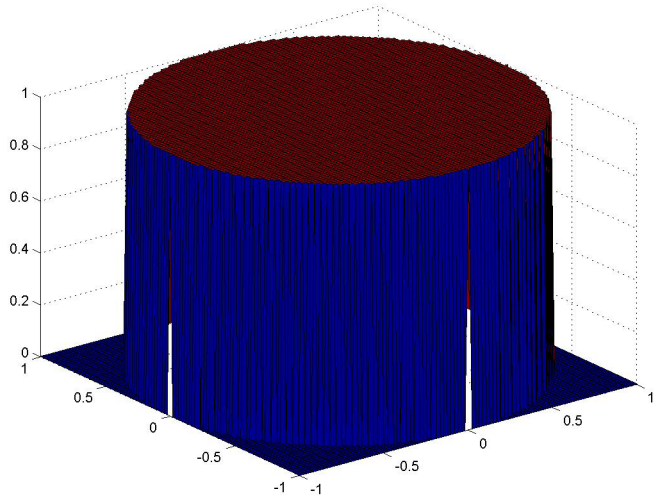

Figure 2.1: Z_0^0: Describes surface mean height.

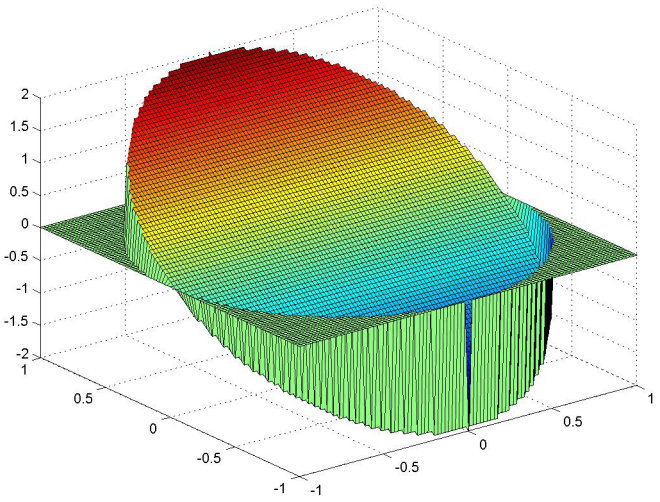

Figure 2.2: Z_1^1: Describes surface tilt, Z_1^{-1} is a 90° rotation of Z_1^1.

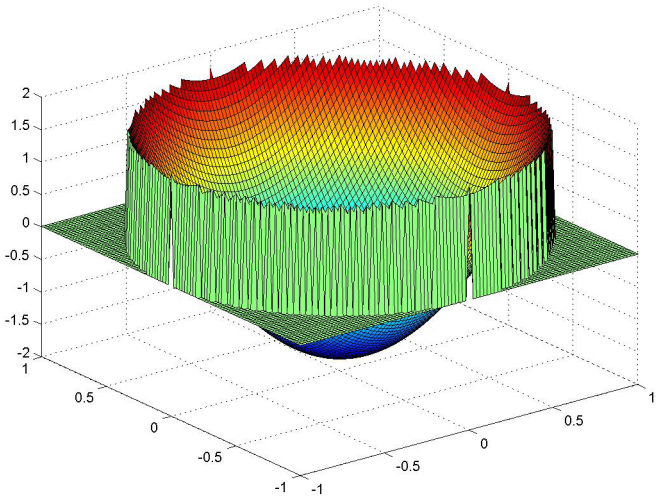

Figure 2.3: Z_2^0: Describes the average curvature of the surface.

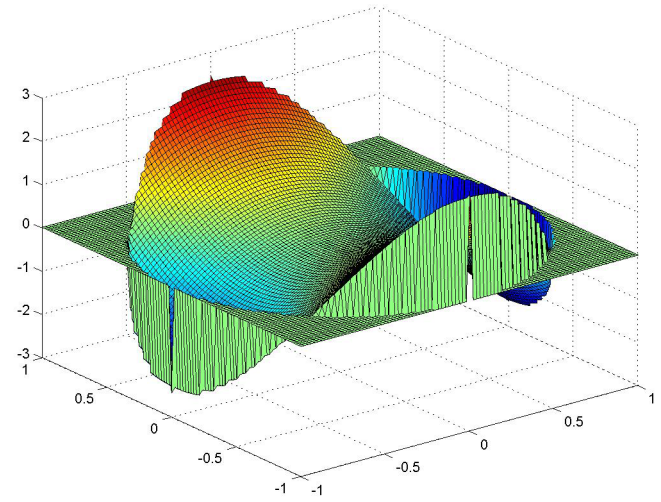

Figure 2.4: Z_2^2: Describes surface astigmatism, Z_2^{-2} is a 45° rotation of Z_2^2.

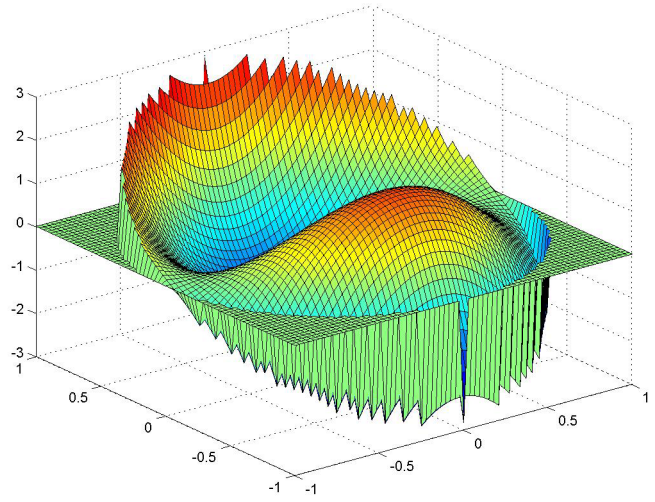

Figure 2.5: Z_3^1: Describes an irregularity structure in surface, Z_3^{-1} is a 90° rotation of Z_3^1.

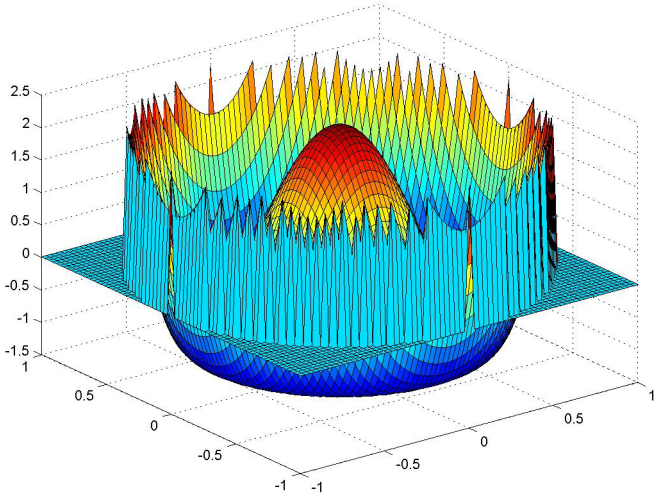

Figure 2.6: Z_4^0: Describes an additional term for the curvature of the surface, also spherical aberration.

determine the surface astigmatism. It is interesting to note the repetition for the non-rotationally symmetric polynomials. For example the Z_1^{-1} is simply Z_1^1 rotated by 90°. This allows the Zernike polynomials to represent a cone on the cornea surface at any orientation. Some of the lower order Zernike polynomials are:

$$Z_0^0(\rho,\theta) = 1, \tag{2.5}$$

$$Z_1^1(\rho,\theta) = 2\rho\cos\theta, \tag{2.6}$$

$$Z_2^0(\rho,\theta) = \sqrt{3}(2\rho^2-1), \tag{2.7}$$

$$Z_2^2(\rho,\theta) = \sqrt{6}\rho^2\cos\theta, \tag{2.8}$$

$$Z_3^1(\rho,\theta) = \sqrt{8}(3\rho^3-2\rho)\cos\theta, \tag{2.9}$$

$$Z_4^0(\rho,\theta) = \sqrt{5}(6\rho^4-6\rho^2+1). \tag{2.10}$$

An important property of the Zernike polynomials is that each coefficient is independent of each other. Considering the corneal surface map, $\Phi(r,\theta)$, has been decomposed into Zernike polynomials,

$$\Phi(r,\theta) = \sum_{n=0}^{\infty}\sum_{m=-n}^{n} a_n^m Z_n^m(r,\theta) \tag{2.11}$$

then each Zernike coefficient (a_n^m) can be found by multiplying $Z_n^m(r,\theta)$ and integrating

over the area.

$$a_n^m = \int_{Area} Z_n^m(r,\theta)\Phi(r,\theta)d\sigma \tag{2.12}$$

Therefore, each coefficient is independent of any other coefficient. Thus by knowing the corresponding coefficients you can uniquely describe a particular visual error. For example, if the astigmatism Zernike coefficients (Z_2^2, Z_2^{-2}, etc.) are determined, then the astigmatism of the system can be uniquely described.

The surface described by a video-keratoscope has a discrete amount of points. Unfortunately, the Zernike polynomials are only orthonormal in the continuous unit circle but not for the discrete case. This can be resolved by applying the Gram-Schmidt orthogonalization procedure to transform the Zernike polynomials into a new set of modified Zernike polynomials $Q_n^m(r)$. The Gram-Schmidt orthogonalization takes a set of nonorthogonal linearly independent functions and constructs an orthogonal set over an arbitrary interval [26]. The same properties hold for the modified Zernike polynomials. By using the Gram-Schmidt orthogonalization procedure, Wang showed that each coefficient can be obtained by back substitution [8]. As a result, the regular least-squares method to determine each coefficient does not have to be used, which may introduce unwanted errors. By using the modified Zernike polynomials, unlike least-squares, each coefficient is independent of the order of the expansion. The modified Zernike polynomials will subsequently be referred to as simply Zernike polynomials.

2.3 Eye Models

To evaluate the optical performance of the human eye, numerous normal eye models have been established and published. Some of the early first-order, or paraxial ($\sin\varphi \approx \varphi$), eye models that are commonly used include the Gullstrand [14] and Von Helmholtz [15] eye models. Conic constants, to simulate aspheric surfaces, were introduced later to improve the eye models. A lens with a gradient refractive index were used in some eye models [18].

Many medical examinations are performed on dilated eyes, and/or a large field angle of detection. Therefore the eye models developed to evaluate the visual acuity and retina image analysis for small pupil sizes are not appropriate for this investigation. Eye models with gradient refractive index for the crystalline lens that greatly increases the complexity of the calculations are also eliminated [18]. Some of the recent eye models that take aberrations into account [16, 17, 18] were evaluated using a ray-tracing computer code [11]. Escudero-Sanz [16] developed an eye model with a field angle up to 60 degrees. Consequently, this normal eye model was adopted for this inquiry. This model takes into account the on-axis and off-axis aberrations that are comparable to real human eye measurements.

Table 2.1 shows the parameters used in the Escudero-Sanz eye model. These parameters are employed in a commercial optics computer code, Zemax^{TM} (ZEMAX Development Corporation, San Diego, CA, USA). The optics computer code is then used to obtain optical ray-tracing calculations that are required to assess the eye's visual

Table 2.1: Geometry of the Schematic Wide-Angle Eye Model[16].

Surface	Type	Conic Constant	Radius (mm)	Thickness(mm)	Optical Medium
1	Conic	-0.26	7.72	0.55	Cornea
2	Spherical	0	6.50	3.05	Aqueous
Stop	Plane	0	Infinity	0	Aqueous
4	Conic	-3.1316	10.20	4.00	Lens
5	Conic	-1.0	-6.00	16.3203	Vitreous
Image	Spherical	0	-12.00		

performance and also to evaluate optical ocular examination instruments. Figure 2.7 illustrates the appearance of a normal model eye.

The refractive indices for each element in this eye model were given at four different wavelengths. Since the human eye is most sensitive around 555 nm, the calculations in this thesis are performed at this wavelength. Whereas the published index of refraction was not provided at 555 nm. Consequently computation of intermediate wavelengths was required. The Conrady formula was used because of its usefulness in fitting sparse data [19].

Refractive errors are simulated by introducing a virtual thin lens at the normal eye model pupil's location. Astigmatic eyes were constructed by inserting different powers in two orthogonal meridians. A KC eye model was created by substituting the normal eye model's outside corneal surface with a KC corneal surface. Therefore, a KC corneal surface model will be constructed in the next section.

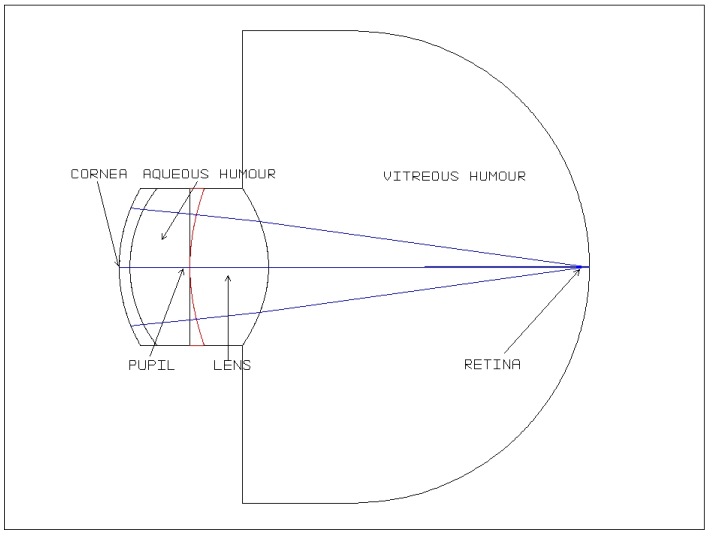

Figure 2.7: Model Eye Used in Ray-Tracing Code.

2.4 Keratoconus Cornea Model

An accurate, or faithful, optical model of KC requires knowledge of the typical values and their ranges of the size, shapes and positions of the conical structures. With the advent of the photo-keratoscope the height map of cornea surface can be determined. The KC cone height is the elevation above a normal corneal surface. Therefore, to reveal the cone's morphology this normal corneal surface should be determined and expunged from the height map. This can be done by decomposing the corneal surface into Zernike polynomials. Accordingly, one eliminates the lower-order polynomials that represent the defocus (near- and far-sightedness) and cylindrical power (astigmatism).

This method was introduced by Schwiegerling to examine the resulting cone from the topographical map [7]. The height maps from KC patients were decomposed into Zernike polynomials up to the fourth order (n=4), then the parabolic ($a_2^0 Z_2^0$), and the

cylindrical ($a_2^2 Z_2^2$ and $a_2^{-2} Z_2^{-2}$) components were eliminated [7, 22]. This results in a residual height map. Corneas with an abnormal curvature and astigmatism will appear as a relatively flat residual map. In this case the cornea's height is closely represented by the parabolic and astigmatic components. Contrary, a KC cornea's residual map will reveal the non-zero higher-order Zernike terms which represent the irregular surface of the cone.

After the cone's surface is obtained the cone's size and corneal position need to be evaluated. This allows an accurate optical KC cornea model to be constructed based on a typical cone parameter's. It is beneficial to represent the KC cone as a model surface shape. Schwigerling used a two-dimensional Gaussian surface to represent the cone [22]. In this thesis the Gaussian cone was also used to simulate the cone with measured values and ranges obtained from Schwigerling [22]. The two-dimensional Gaussian function is represented by:

$$f(x,y) = h_0 \exp -[\frac{(x-x_0)^2}{2\sigma_x^2} + \frac{(y-y_0)^2}{2\sigma_y^2}], \tag{2.13}$$

where h_0 is the peak height of the cone, (x_0, y_0) is the cone's center location, and σ_x and σ_y are the horizontal and vertical dimensions where the height drops to $e^{-\frac{1}{2}}$ of the cone's peak height. Schwigerling matched the two-dimensional Gaussian parameters (x_0, y_0, σ_x, σ_y, h_0) to fifty-six clinically diagnosed KC patient residual height maps (three mild, forty-five moderate, and eight severe cases). Each parameter's statistical distribution reported by Schwigerling is discussed further in section 3.2.

These five different parameters, along with their distributions, are used in this inves-

tigation to simulate various KC cone dimensions and locations. A synthetic KC corneal surface is generated by superimposing the KC cone onto a normal corneal surface. The synthetic KC corneal surface can be replaced in the normal eye model's corneal surface, (section 2.3). In this way a KC eye model is obtained. The irregular exterior corneal surface cannot be directly modeled using a standard Zemax surface. Therefore the five cone parameters and the normal eye model's corneal radius and conic constant are used to create the artificial KC corneal surface. Microsoft Visual C++ is used to create the KC corneal surface file required to produce the non-standard Zemax surface.

The surface generated by the C++ code is an intuitive KC corneal model. The synthetic KC cornea is created by superimposing a typical KC cone onto the exterior corneal surface from the Escudero-Sanz normal eye model [16]. The KC cone is modeled using the range of measured cone parameters obtained by Schwigerling [22]. Although the interior corneal surface is affected in KC patients the visual significance is not as great. This is in view of the fact that the index of refraction difference is small between the cornea and aqueous humour mediums. The KC eye model is used to investigate the visual performance in Chapter 3, and to evaluate the detection capabilities of optical instruments in Chapter 4. Figures 2.8 and 2.9 illustrate the 3-D profile and 2-D contour shape of a KC cone modeled using the two dimensional Gaussian function.

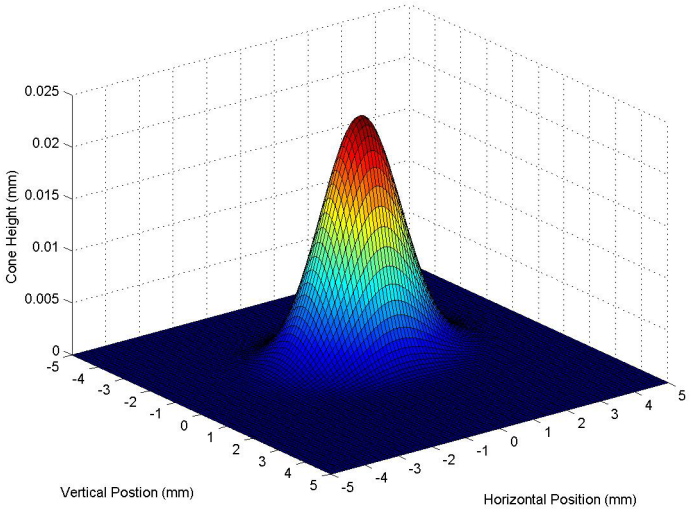

Figure 2.8: Typical 3-Dimensional View of Modeled Keratoconus Cone.

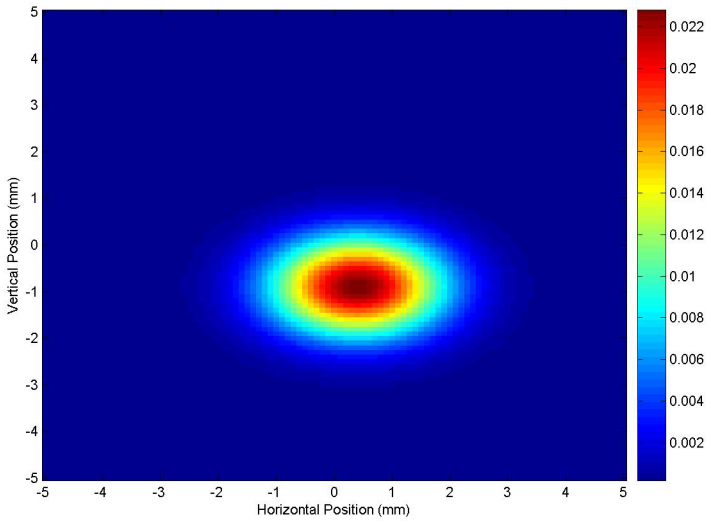

Figure 2.9: Typical 2-Dimensional View of Modeled Keratoconus Cone.

Chapter 3

Keratoconus Eye Visual Performance

There is currently little information on how the KC cone affects the eye's visual performance. One method to evaluate the visual performance is to determine the equivalent refractive error, and the effectiveness of eye spectacles. By examining a KC eye's wave-front aberration the equivalent refractive errors can be established. The spectacles effectiveness to correct the vision can be obtained by examining the remaining wave-front aberration. Then by constructing different KC cones the characteristics that affect the vision significantly can be obtained. For each different cone characteristic a refractive error analysis will be performed.

3.1 Evaluating Visual Performance Through Wave Front Aberration

To evaluate the visual performance of KC eyes the equivalent refractive errors for different degrees of KC needs to be calculated. This is accomplished by determining the corresponding equivalent clinical KC eye prescription. The equivalent eye prescription, in plus-cylinder form, gives the spherical power (Φ), cylindrical power (Φ_a), and the corresponding angle describing the astigmatism axis (θ_a). An astigmatic eye consists of two perpendicular meridians specifying the maximum and minimum powers (curvatures). In plus-cylinder interpretation, the spherical power is the minimum power in one meridian. The cylindrical power is the difference of the two (maximum and minimum) spherical powers. The astigmatism axis specifies the rotation about the optical axis to determine the cylindrical meridian location. There are two different ways to represent the eye prescription, plus-cylinder and minus-cylinder form. If the prescription is written in plus-cylinder form as $(\Phi_{min}, \Phi_a, \theta_a)$ the corresponding minus-cylinder form is written as $(\Phi_{max}, -\Phi_a, \theta_a + 90^\circ)$.

The model KC eye's equivalent refractive error is determined by examining the wave front aberration (WFA). WFA is defined as the optical path difference (OPD) between the real wave front and a reference, or perfect wave front, as a function of position on the exit pupil. The wave front aberration is a useful tool to evaluate an ocular system's visual performance. A wave front is a surface described with equal phases. The wave front of a point source in space is a sequence of spherical surfaces moving outward.

The two dimensional WFA function can be expanded into any orthogonal complete functions. The Zernike polynomials are typically used. As is discussed in chapter 2.2, the Zernike polynomials have useful features in optometry and recently have gained considerable popularity in the vision science community. The wave front of a perfect eye with a point source located at the retina will emerge as a plane-wave. As shown in Fig 3.1, the WFA of an eye can be measured experimentally by projecting a laser beam onto the retina to form a diffusive point source. The rays from the point source travel through the eye's elements and exit the cornea. The 2-dimensional wave front at the exit pupil is determined and compared with an ideal wave front, a plane wave in this case, to obtain the point to point difference. The point to point difference is described as $W(\rho, \theta)$, where $\rho = r/r_{max}$ is the normalized exit pupil radius, and θ is the azimuthal angle. The wavefront aberration is usually expressed in units of microns μm or wavelengths λ. It is helpful to apply the wavelength to describe the WFA since destructive interference occurs when $W(\rho, \theta) > \frac{\lambda}{2}$. Normally the WFA is assigned to be zero at the center point, $W(\rho = 0) = 0$.

The cornea's refractive prescription was previously found by Schwiegerling using Zernike polynomials [7]. The mean power and astigmatism have also been found from the wavefront using Zernike polynomials [27]. The Schwiegerling method is modified to evaluate the whole eye's prescription, since this is what an ophthalmologist would measure in the clinic. Therefore, only a short description will be discussed here, and the changes made will be noted.

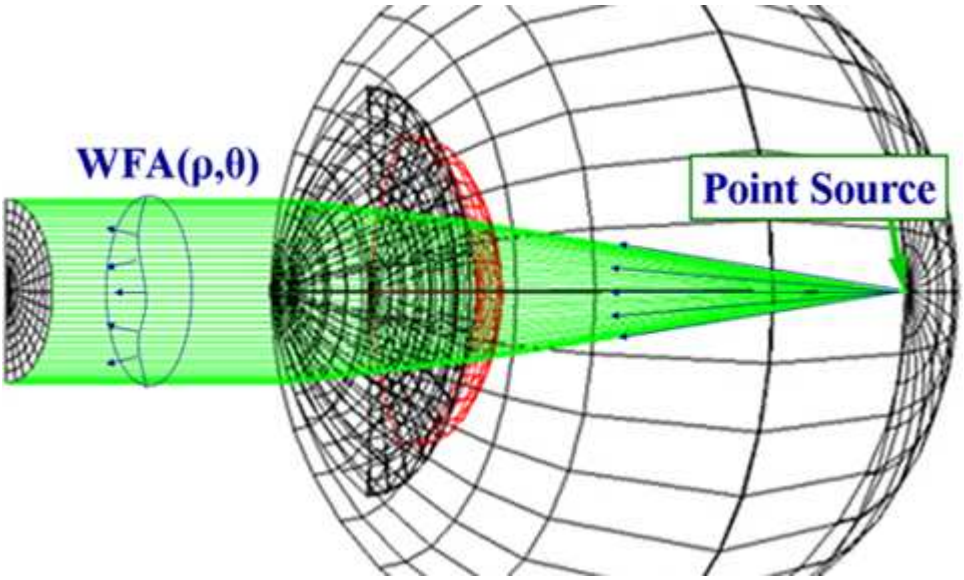

Figure 3.1: Eye's Wave Front Aberration.

To evaluate the prescription, the total eye's WFA function needs to be decomposed into Zernike polynomials, as described in section 2.2. Once the WFA has been decomposed, the spherical power, astigmatism power, and astigmatism axis can be determined. The astigmatism axis can be established by finding the extremum of the Zernike astigmatism terms Z_2^2 and Z_2^{-2}. The axis is obtained by taking the derivative and equating it to zero, then solving for θ. The astigmatic axis is then represented in terms of Zernike astigmatism coefficients.

$$\theta_0 = \frac{1}{2} \arctan \frac{a_2^{-2}}{a_2^2} \tag{3.1}$$

There exists two solutions $\theta = \theta_0$ and $\theta = \theta_0 + 90^\circ$ that satisfy the equation. Therefore

the astigmatic axis is given by

$$\begin{aligned} \theta_a &= \theta_0 && \text{for } a_2^{-2}\sin 2\theta_0 + a_2^2 \cos 2\theta_0 < 0 \\ &= \theta_0 + 90^\circ && \text{for } a_2^{-2}\sin 2\theta_0 + a_2^2 \cos 2\theta_0 > 0 \end{aligned} \tag{3.2}$$

If the astigmatic axis is negative then 180° is added so that the range is $0 \leq \theta_a < 180^\circ$.

The spherical and cylindrical powers are obtained by equating the Zernike parabolic terms, up to the fourth order, to the wavefront's spherical sag. An approximation of the spherical sag is defined as:

$$sag = \frac{\rho^2 r_{max}^2}{2R_0} \tag{3.3}$$

where $\rho = \frac{r}{r_{max}}$, r_{max} is the exit pupil's radius (determined from optical software), r is the radial coordinate, and R_0 is the sphere's curvature radius. It was determined [7] that the two solutions $R_0 = R_\perp$ for $\theta = \theta_0$ and $R_0 = R$ for $\theta_0 + 90^\circ$ are:

$$R_\perp = \frac{r_{max}^2}{2[2\sqrt{3}a_2^0 - 6\sqrt{5}a_4^0 + \sqrt{6}(a_2^2\cos 2\theta_0 + a_2^{-2}\sin 2\theta_a) - 3\sqrt{10}(a_4^2\cos 2\theta_0 + a_4^{-2}\sin 2\theta_0)]}. \tag{3.4}$$

Similarly, for $\theta = \theta_0 + 90^\circ$:

$$R = \frac{r_{max}^2}{2[2\sqrt{3}a_2^0 - 6\sqrt{5}a_4^0 - \sqrt{6}(a_2^2\cos 2\theta_0 + a_2^{-2}\sin 2\theta_a) + 3\sqrt{10}(a_4^2\cos 2\theta_0 + a_4^{-2}\sin 2\theta_0)]}. \tag{3.5}$$

The two orthogonal powers in diopters can be determined, if the units are mm, from:

$$\Phi_{\perp} = \frac{1000}{R_{\perp}}, \tag{3.6}$$

and

$$\Phi = \frac{1000}{R}. \tag{3.7}$$

The cylindrical power Φ_a is given by

$$\Phi_a = \Phi_{\perp} - \Phi. \tag{3.8}$$

There is a sign change since the power to correct the eye is required. To determine the power in the principal meridians requires an infinite number of ρ^2 terms. Only the Zernike terms up to the fourth order ($n = 4$) were used to calculate the powers in the two meridians.

The higher-order aberrations cannot be represented by the spherical and cylindrical powers. Spectacles alone cannot correct these higher-order aberrations. Therefore, a value to determine the higher-order aberrations significance is constructed. To represent the higher-order aberrations the $W_{3,4}$ value is introduced. The $W_{3,4}$ is defined as

$$\begin{aligned} \text{RMS of } WFA_{HO} &= \int\int W^2_{n\geq 3} \rho d\theta d\rho, \\ &= \sqrt{\sum_{n=3}^{\infty} \sum_{m=-n}^{m=n} (a_n^m)^2}, \end{aligned}$$

$$\begin{aligned} &\approx \sqrt{\sum_{n=3}^{4}\sum_{m=-n}^{m=n}(a_n^m)^2}, \\ &= W_{3,4}, \end{aligned} \tag{3.9}$$

where the RMS of WFA_{HO} represents the root mean square (RMS) of the higher order wave front terms ($n \geq 3$), and a_n^m represent the Zernike polynomial coefficient. Only the $n = 3, 4$ terms are included because they are the most consequential. Now the higher order aberrations are approximated by the $W_{3,4}$ value.

3.2 KC Eye Visual Performance Analysis

As was discussed in section 1.3, KC is commonly classified by the degree of dioptric power or the cone's shape. Little is known as to how the cone's characteristics affect the dioptric power. In this section the KC eye model is used to simulate different degrees of KC. Cone parameters that affect the vision significantly are found after examining their optical effects. Then the KC visual affects are evaluated for each distinctive KC cone parameter.

Four KC eye degrees (mild, moderate, advanced, and severe) are created. Each degree is based on Schwiegerling's fifty-six measured cones statistical distribution. These four KC classification degrees do not have a direct correspondence with Table 1.1.

Figures 3.2, 3.3, 3.4, and 3.5 illustrate each measured cone's distribution of size, volume, and location from Schwiegerling [22]. Three cones are randomly generated for each or the four different KC degrees. Two additional round cones are generated, since none were randomly produced. Table 3.1 gives the characteristic variables describing the fourteen KC cones . The cone variables include: peak height (h_0), horizontal and vertical radius (σ_x and σ_y), volume, and the shape (eccentricity). The cones are numbered according to an increase in the peak height. The 2-D Gaussian surface volume (V) is given by

$$V = 2\pi h_0 \sigma_x \sigma_y. \tag{3.10}$$

The shape or eccentricity (e) is given by the ellipse equation

$$e = \sqrt{1 - \frac{b^2}{a^2}}, \tag{3.11}$$

where b is the semi-minor axis ($min[\sigma_x, \sigma_y]$), and a is the semi-major axis ($max[\sigma_x, \sigma_y]$). An eccentricity $e = 0$ corresponds to a round shaped cone, while $e = 1$ corresponds to a line, using this definition of a and b.

Figure 3.6 illustrates the fourteen chosen cones in a false colored image. Each image is 10 mm in diameter, and the max height is 55 μm for the most severe cone. Cone #7 and #11 represent the round cones added to the randomly shaped elliptical cones. Cones # 1-3 represent the mild, # 4-7 moderate, # 8-11 advanced, and # 12-14 severe KC cones.

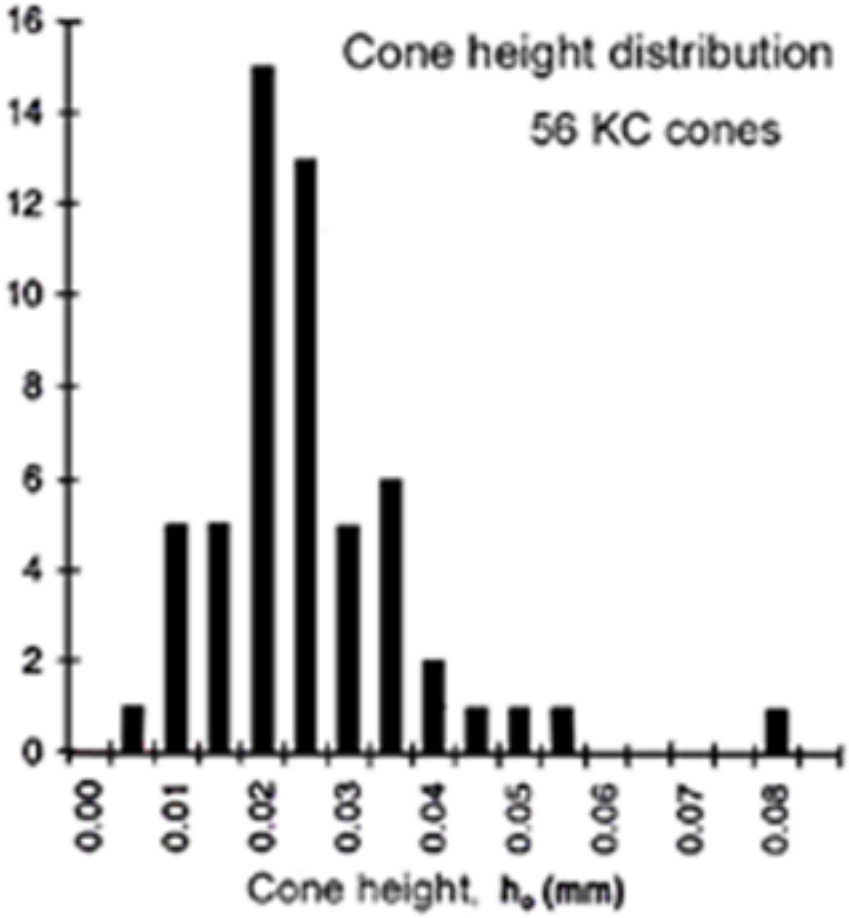

Figure 3.2: Measured Cone Height Distribution [22].

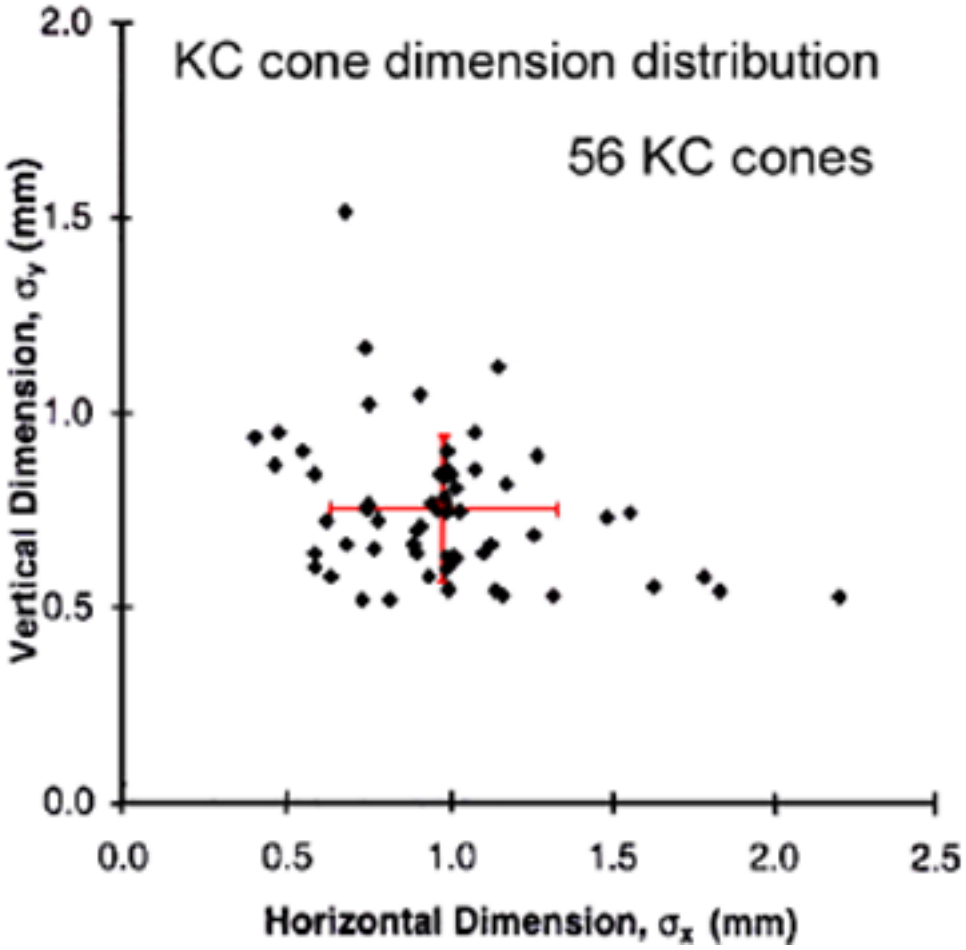

Figure 3.3: Measured Cone Dimension Distribution. The red cross shows the mean value and standard deviations.[22].

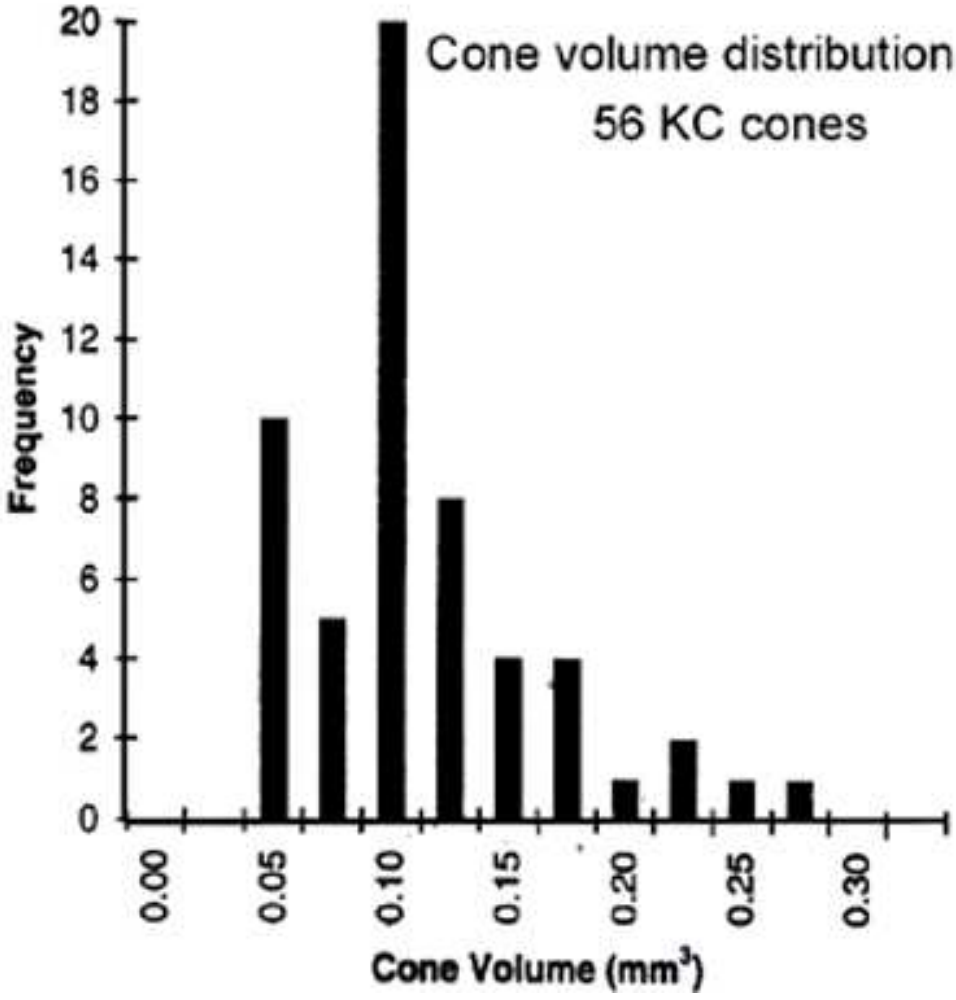

Figure 3.4: Measured Cone Volume Distribution [22].

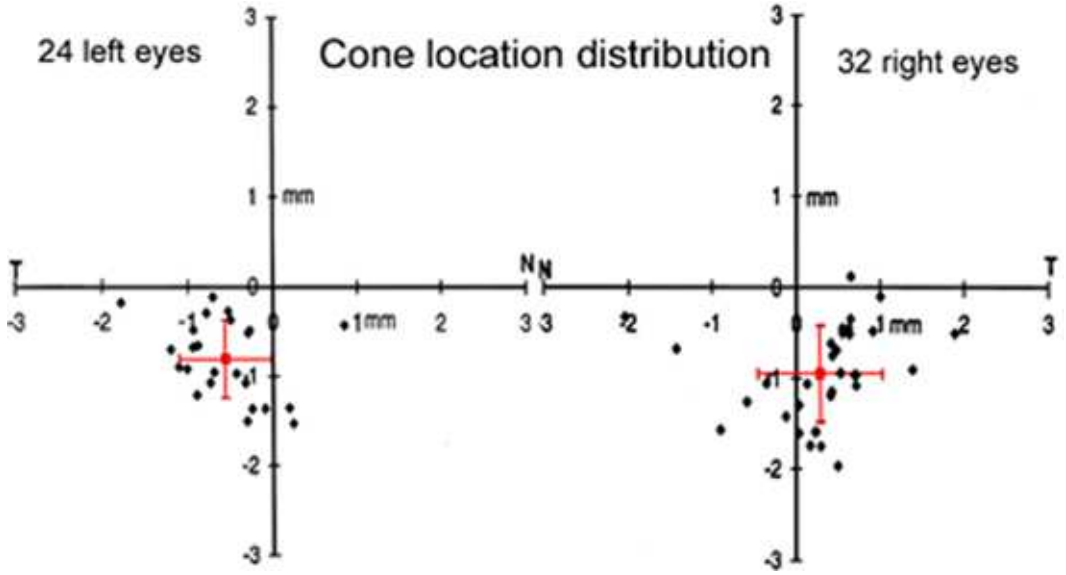

Figure 3.5: Measured Cone Location Distribution, T and N indicate the temporal and nasal directions. The red symbols and crosses in the 2 plots indicate the mean locations and standard deviations of the distributions. [22].

Table 3.1: Keratoconus Cone Parameters.

KC Degree	Cone #	h_0 (mm)	σ_x (mm)	σ_y (mm)	Volume (mm^3)	Eccentricity (e)
mild	1	0.0051	0.418	0.473	0.0146	0.282
	2	0.0087	0.435	0.572	0.0136	0.649
	3	0.0090	0.517	0.496	0.0063	0.467
moderate	4	0.0101	0.732	0.694	0.0323	0.317
	5	0.0118	0.658	0.775	0.0380	0.529
	6	0.0156	0.642	0.601	0.0377	0.351
	7	0.0200	0.800	0.800	0.0804	0.000
advanced	8	0.0246	1.182	0.855	0.1561	0.690
	9	0.0269	0.970	0.882	0.1447	0.415
	10	0.0296	1.161	0.882	0.1907	0.650
	11	0.0400	1.200	1.200	0.3619	0.000
severe	12	0.0410	1.738	1.059	0.4746	0.729
	13	0.0507	1.701	1.028	0.5568	0.797
	14	0.0541	1.762	1.031	0.6180	0.811

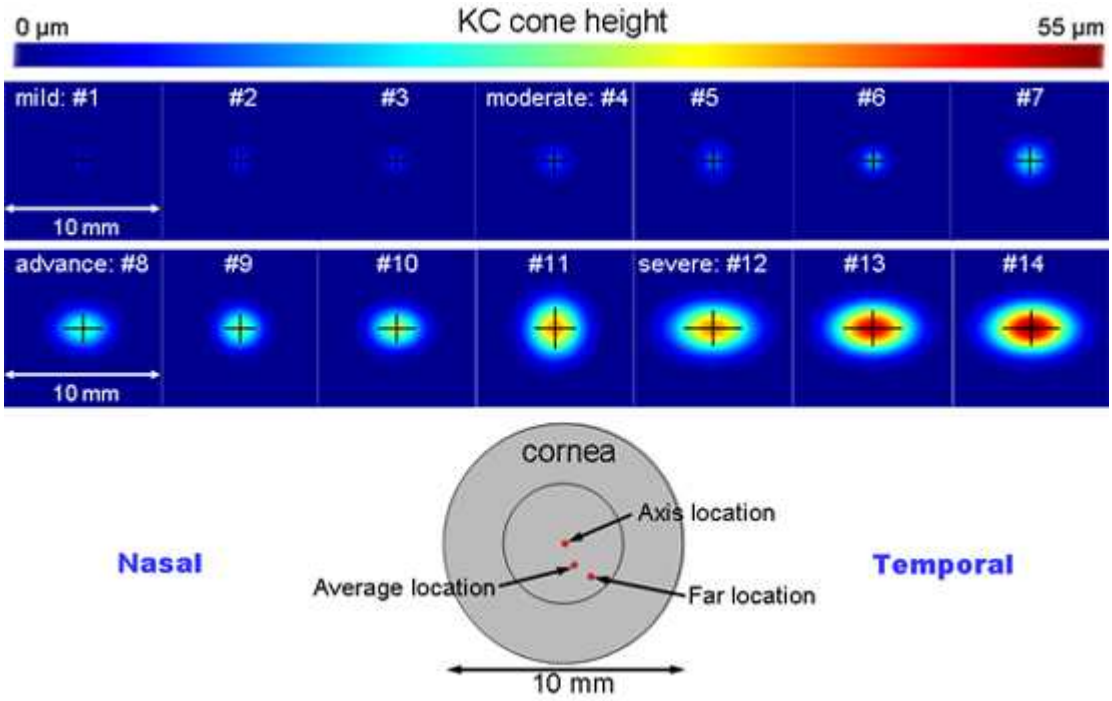

Figure 3.6: 14 Synthetic KC Cones Describing 4 Degrees (mild, moderate, advanced, and severe). The lower portion illustrates three cone locations on the cornea used during the calculations.

Table 3.2: 14 Keratoconus on Axis: Equivalent Prescription.

Cone #	Spherical Eq. Power (D)	Cylindrical Power (D)	Axis (degrees)	$W_{3,4}$ (μm)
1	-2.99	0.29	180	0.21
2	-5.24	1.38	180	0.38
3	-5.52	0.23	180	0.39
4	-5.26	0.41	180	0.30
5	-6.16	1.49	180	0.36
6	-9.00	0.77	180	0.58
7	-9.26	0.00	180	0.50
8	-8.55	4.83	180	0.43
9	-10.35	1.70	180	0.49
10	-10.17	4.92	180	0.49
11	-10.20	0.00	180	0.35
12	-9.24	8.21	180	0.41
13	-12.04	10.84	180	0.51
14	-12.62	12.01	180	0.61

To determine each cone's visual affect the spherical equivalent power (SE), cylindrical power, astigmatism axis, and the RMS of the higher-order WFA is evaluated. The method to obtain the two orthogonal spherical powers and cylindrical power is discussed in section 3.1. The spherical equivalent (SE) is the average of the two orthogonal spherical powers. A positive (negative) SE indicates an average far- (near-) sighted eye. The SE and cylindrical refractive errors can be corrected with normal eye spectacles. However, $W_{3,4}$ represents the higher order aberrations that cannot be corrected with spectacles. The 14 KC eye's equivalent prescription is given in Tables 3.2, 3.3, and 3.4, corresponding to the three different cone locations. The three different cone locations (on visual axis: $x_0 = 0.0$, $y_0 = 0.0\ mm$, average location: $x_0 = 0.404$, $y_0 = -0.891\ mm$, and far location: $x_0 = 1.079$, $y_0 = -1.385\ mm$) selected are based on the measured locations from Schwigerling, shown in lower portion of figure 3.6.

The pupil's diameter also influences the WFA, and thus the visual performance is

Table 3.3: 14 Keratoconus Average Location: Equivalent Prescription.

Cone #	Spherical Eq. Power (D)	Cylindrical Power (D)	Axis (degrees)	$W_{3,4}$ (μm)
1	0.17	-2.48	114	0.26
2	-0.18	-4.18	114	0.46
3	0.29	-4.46	114	0.47
4	-0.56	-3.77	114	0.45
5	-1.19	-4.45	114	0.53
6	-0.26	-6.84	114	0.77
7	-1.90	-6.20	114	0.79
8	-1.82	-4.10	119	0.81
9	-2.76	-5.99	115	0.89
10	-2.48	-4.90	118	0.93
11	-5.04	-4.56	114	0.79
12	-3.29	2.00	143	0.95
13	-3.98	2.67	143	1.24
14	-4.14	2.59	144	1.33

Table 3.4: 14 Keratoconus Far Location: Equivalent Prescription.

Cone #	Spherical Eq. Power (D)	Cylindrical Power (D)	Axis (degrees)	$W_{3,4}$ (μm)
1	0.25	-0.44	130	0.16
2	0.55	-1.20	132	0.29
3	0.54	-1.17	127	0.29
4	0.82	-2.47	127	0.30
5	0.93	-2.97	131	0.36
6	1.21	-3.19	127	0.49
7	1.42	-5.21	128	0.54
8	1.48	-5.85	121	0.51
9	1.49	-6.78	126	0.61
10	1.60	-6.99	122	0.61
11	0.08	-7.40	128	0.65
12	0.88	-6.18	119	0.67
13	1.38	-8.13	119	0.85
14	1.47	-8.41	118	0.91

also affected. A three mm pupil diameter is chosen to evaluate the visual performance during this chapter. Figure 3.7 also illustrates the normal refractive errors (SE and absolute cylindrical) for the fourteen cones at the three different locations. The absolute cylindrical (AC) is the magnitude of the cylindrical power.

Interpreting the optical affects shown in Tables 3.2, 3.3, 3.4 and Figure 3.7 give an idea into which cone parameters significantly affect the eye's vision. In Figure 3.7 the on-axis cones (yellow points) have a much larger near-sighted power than cones further from the visual axis. The on-axis cone's shape also has a significant refractive error effect. This can be seen by examining the examining the specific on-axis cones #7 and #11 in Figure 3.7. These round cones have no cylindrical power. While the oval cones have an increased AC. The cone's dimension (volume) also seems to have a refractive error affect. As the on-axis cone's dimension increases the SE becomes more near-sighted. The higher order terms in the WFA ($W_{3,4}$) are smaller for on-axis cones. This is observed by comparing Table 3.2 with Tables 3.3 and 3.4. Although the on-axis cones have the greatest dioptric powers, they are corrected with normal spectacles better than can the off-axis cones

At the average location (green points) the SE power is more far-sighted. When the cones are moved to the far location (blue points) the SE becomes positive, resulting in a far-sighted eye. For both locations the higher order WFA terms increase as the dimension increases. The far location's high order WFA terms are smaller than the average location's. The shape affect appears less significant for cones at the average

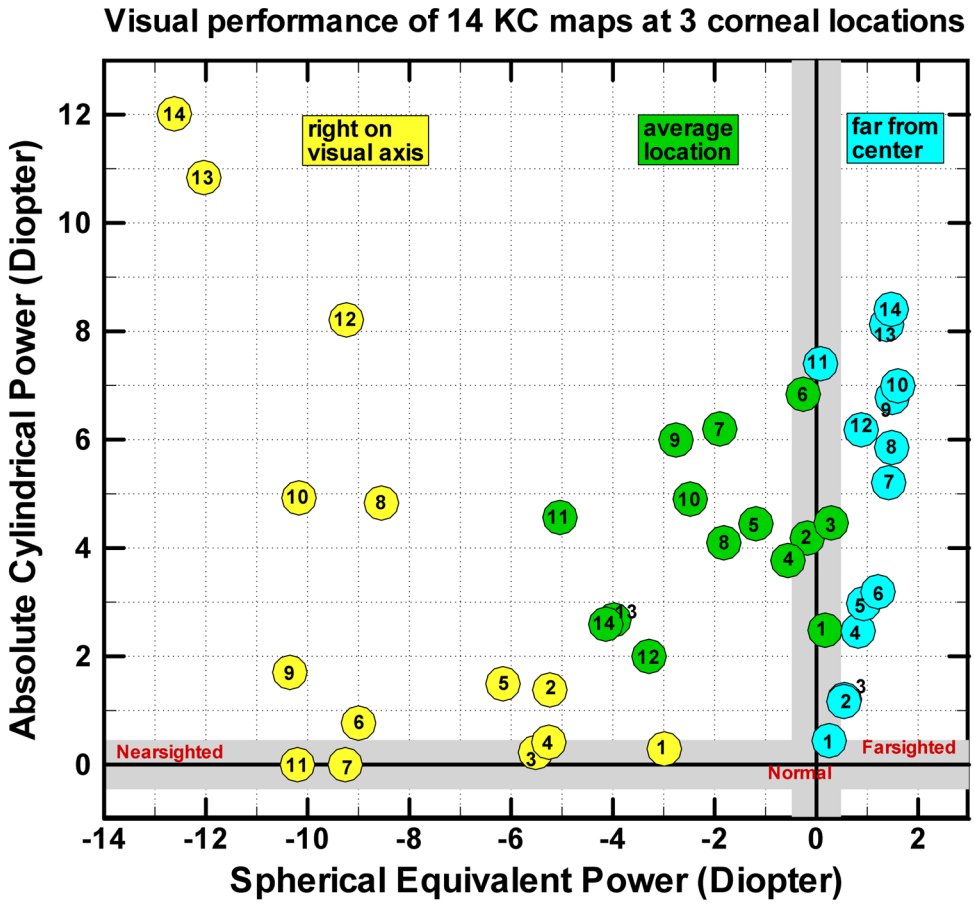

Figure 3.7: Keratoconus Normal Refractive Errors For 14 Different Cones at 3 Different Locations.

and far location. Unlike the on-axis round cone's there is always a cylindrical power present away from the visual axis.

It can be seen by comparing Table 1.1 with these results that only the cones near the visual axis correspond to the more severe cases of KC. Three different cone parameters are studied to determine how the KC cone affects the visual performance. Related to the previous discussion, the cone parameters chosen are: distance from visual axis, dimension, and shape. The cone's visual performance is considered individually during the remaining sections.

3.3 Cone Location Visual Affects

Possibly the most important cone parameter that notably affects the vision is the cone's apex location. To determine the cone location affects three cones are analyzed. The three cones represent a small ($h_0 = 0.008$, $\sigma_x = 0.5$, $\sigma_y = 0.5\ mm$), medium ($h_0 = 0.02$, $\sigma_x = 0.8$, $\sigma_y = 0.8\ mm$), and a large ($h_0 = 0.05$, $\sigma_x = 1.5$, $\sigma_y = 1.5\ mm$) round cone. This ensures that the cone's shape does not affect the prescription. Each cone is moved radially outward from the optical center to a final radius of 3.5 mm. The path is directed along an angle of 45° below the horizontal axis.

Figure 3.8 illustrates the three different cone's location prescription effects. This figure demonstrates how the cone's location affects the spherical equivalent, cylindrical, and higher-order aberrations. The cone's curvature determines the spherical power. The cone's curvature is found by taking the laplacian of the gaussian function, Eq. 3.12.

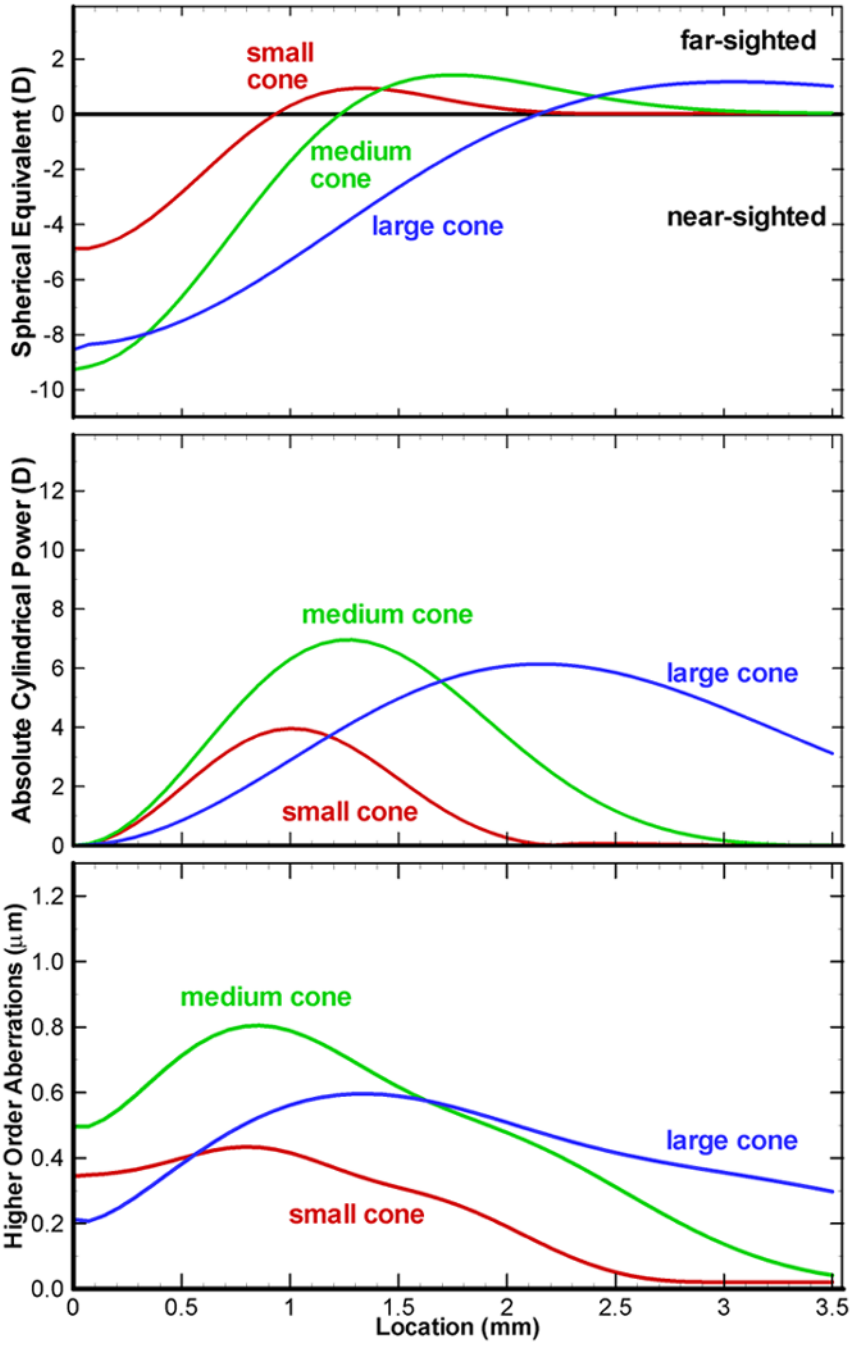

Figure 3.8: Keratoconus Cone Location Visual Prescription Affects. Top: Spherical Equivalent Power. Middle: Absolute Cylindrical Power. Bottom: Root-mean-square of higher-order aberrations $W_{3,4}$.

Figures 3.9, 3.10, and 3.11 demonstrate the three different cone's curvature.

$$\begin{aligned} \bigtriangledown^2 f(x,y) &= \frac{h_0 x^2 \exp[-(\frac{x^2}{2\sigma_x^2}+\frac{y^2}{2\sigma_y^2})]}{\sigma_x^4} - \frac{h_0 \exp[-(\frac{x^2}{2\sigma_x^2}+\frac{y^2}{2\sigma_y^2})]}{\sigma_x^2} \\ &+ \frac{h_0 y^2 \exp[-(\frac{x^2}{2\sigma_y^2}+\frac{y^2}{2\sigma_y^2})]}{\sigma_x^4} - \frac{h_0 \exp[-(\frac{x^2}{2\sigma_x^2}+\frac{y^2}{2\sigma_y^2})]}{\sigma_y^2} \end{aligned} \tag{3.12}$$

There are several visual effects obtained from Figs. 3.8, 3.9, 3.10, and 3.11. Fig. 3.8 illustrates that the small (red lines) and average (green lines) sized cones have little or no spherical equivalent, cylindrical power, or $W_{3,4}$ far from the axis. The large (blue lines) cone prescriptions still exist at 3.5 mm. Near the visual axis, each cone's higher-order aberrations increase as the distance from the visual axis increases. Then the higher-order aberrations reach a maximum and then gradually decrease until they are insignificant. The refractive error prescription changes can also be seen from the cone's curvature. The small (Fig. 3.9) and medium (Fig. 3.10) cone's curvature rapidly changes, and then becomes insignificant far from the visual axis. Whereas the large (Fig. 3.11) cone's curvature changes less drastically, and is gradually decreasing to zero.

From Fig 3.8 the smaller cones near the visual axis apex have an increased negative SE power (near-sightedness). As the distance increases the power switches and becomes positive (far-sightedness) before going to zero. The large cone's SE power changes also, but is not zero at 3.5 mm. These effects can also be observed from the cone's curvature. For each cone the curvature's concavity changes sign near the location where the SE

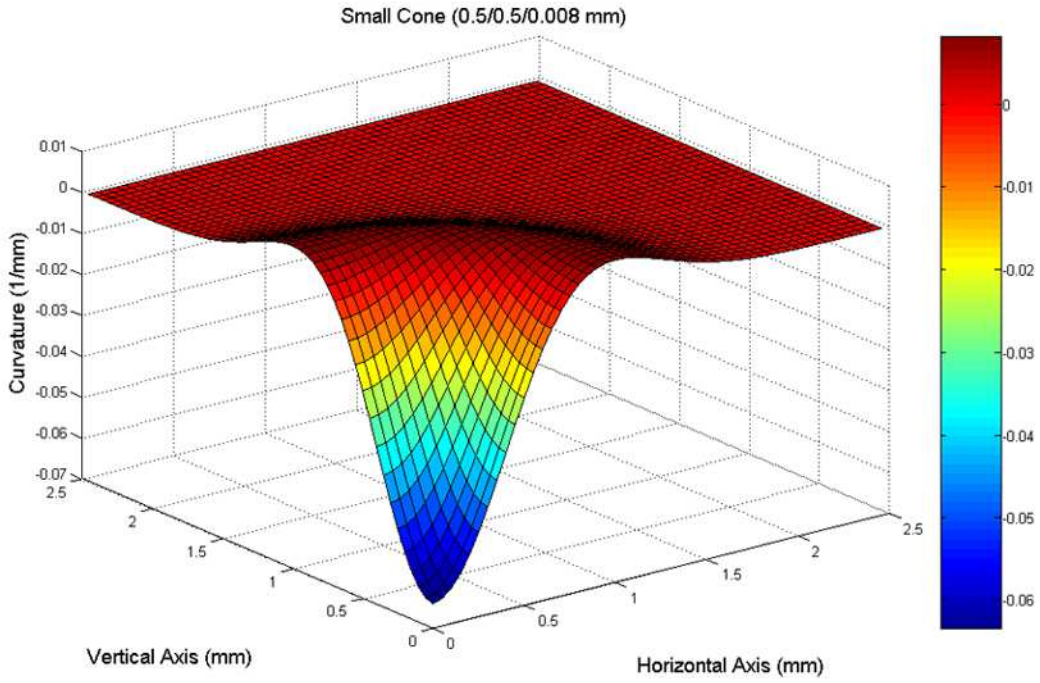

Figure 3.9: Surface Curvature For Small Cone ($\sigma_x/\sigma_y/h_0$).

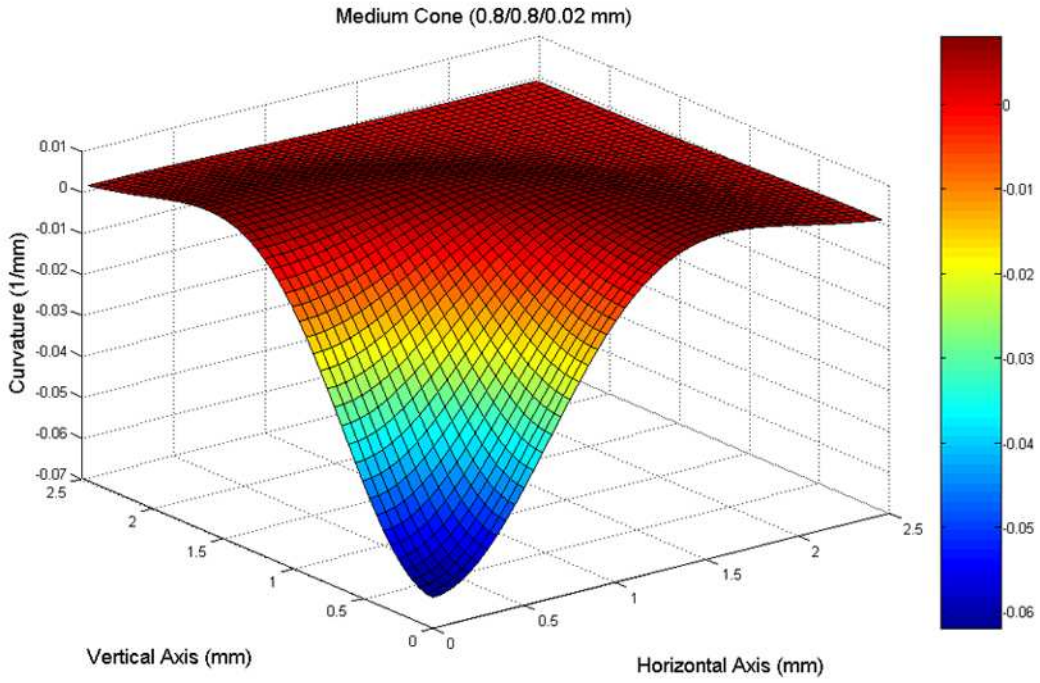

Figure 3.10: Surface Curvature For Medium Cone ($\sigma_x/\sigma_y/h_0$).

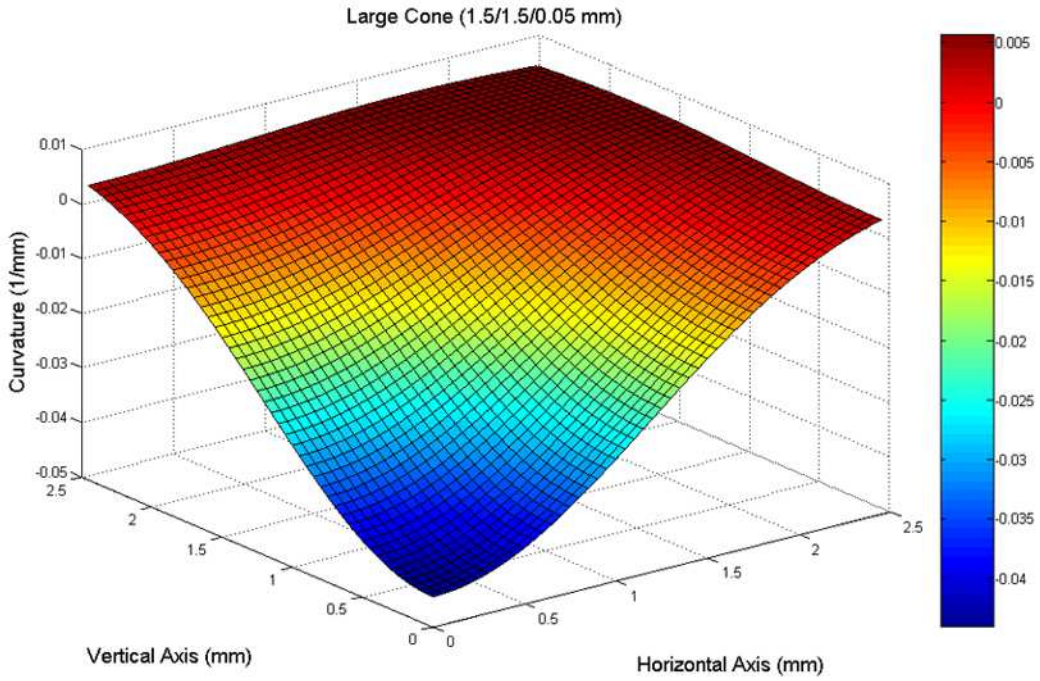

Figure 3.11: Surface Curvature For Large Cone ($\sigma_x/\sigma_y/h_0$).

power changes sign. The curvature switching signs causes a particular region to change from convex to concave. When this region is near the visual axis the eye switches power. The maximum absolute cylindrical power is greatest when the SE is zero, or when the curvature concavity changes near the visual axis. Therefore from these observations, it seems the corneal curvature near the visual axis has a significant dioptric effect.

3.4 Cone Dimension Visual Affects

The cone's dimension, or volume, also remarkably affects the vision. Three different cone locations are applied to understand how the cone dimension affects the equivalent prescription. The cone's apex is located on the visual axis ($x_0 = 0.0$, $y_0 = 0.0\ mm$), at the average location ($x_0 = 0.404$, $y_0 = -0.891\ mm$), and at a far location ($x_0 = 1.079$, $y_0 = -1.385\ mm$). Each cone has the same h_0, σ_x, and σ_y ratio ($\frac{h_0}{h_0} = 1 : \frac{\sigma_x}{h_0} = 42.4 : \frac{\sigma_y}{h_0} = 32.6$). Then the cone's height (h_0) is varied from 0.002 to 0.1 mm by 0.002 mm, and the other cone characteristics are determined from the constant ratios. This results in each cone having the same shape, even though the volume is increased.

Figure 3.12 demonstrates the equivalent prescription changes for on axis, average, and far located similarly shaped cones. The average and far located cones exhibit alike prescription behavior. The only difference is that the closer cones have a greater spherical equivalent power, and less higher-order aberrations. Both cone locations are far-sighted for smaller dimensions. As the dimension increases the eye proceeds to become more near-sighted.

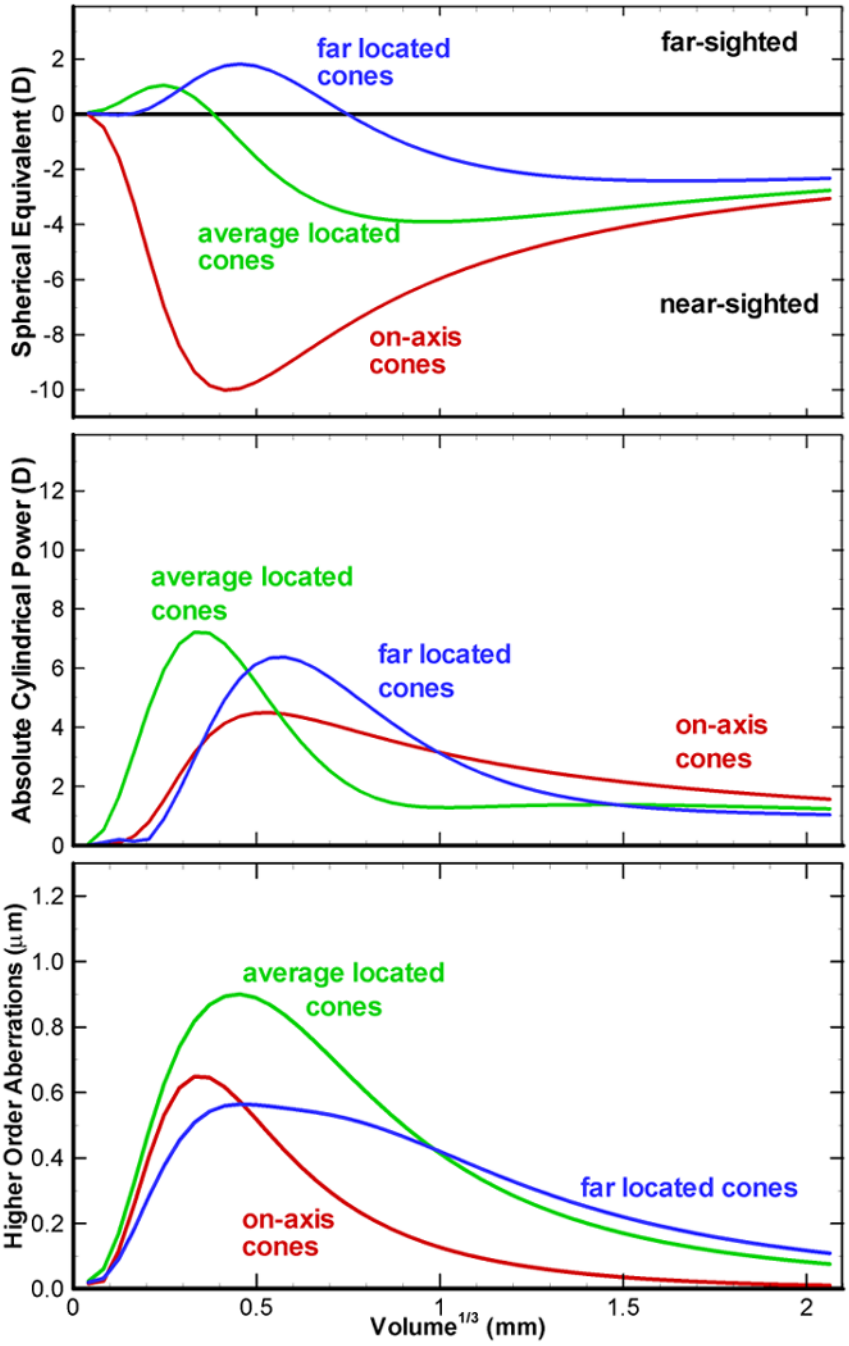

Figure 3.12: Keratoconus Cone Dimension Visual Prescription Affects. Top: Spherical Equivalent Power. Middle: Absolute Cylindrical Power. Bottom: Root-mean-square of higher-order aberrations $W_{3,4}$.

This in view of the fact that both meridian powers are the same sign, while for smaller dimensions they are different. The absolute cylindrical power also increases for smaller dimensions. The maximum cylindrical occurs as the cone's boundary (σ) approaches the visual axis center.

The cones located at the visual axis behave entirely different. As the dimension increases the near-sightedness rapidly increases until it reaches about ten diopters. Then for larger dimensions the near-sighted SE gradually decreases to about three diopters. This implies that although the dimension increases the spherical equivalent becomes less significant. This can be explained by examining the cone curvature. As the dimension increases the cone becomes broader which causes little curvature change. In contrast, as the cone's dimension decreases the peak sharpens, which creates faster curvature changes . The higher-order aberrations are much larger for smaller cone dimensions, and the average located cones have the largest higher-order aberrations. The largest cone dimensions have comparable equivalent prescriptions for each location. This implies that all cones far from the visual axis have similar prescriptions.

3.5 Cone Shape Visual Affects

The last cone parameter that greatly affects the vision is the cone's shape. To demonstrate how the shape parameter affects the eye's prescription three different locations are examined. Each cone has the same volume ($V = 0.12\ mm^3$), and the σ_x and σ_y ratio are varied from $\frac{\sigma_x}{\sigma_y} = 2.5$ to $\frac{\sigma_x}{\sigma_y} = \frac{1}{2.5}$. The natural logarithm of the ratio is used

during the calculations because the shape can be varied evenly from $\ln \frac{1}{2.5} = 0.916$ to $\ln 2.5 = -0.916$.

Figure 3.13 illustrates how the cone's shape can affects the eye's equivalent prescription. The three elliptical shapes at the figure's bottom illustrate how the cone's shape changes for different ratios. The figure's horizontal axis represents the shape as the $\ln \frac{\sigma_x}{\sigma_y}$. The on axis cone's shape has the greatest cylindrical power effect of all the cone parameters. The round cone on axis has no cylindrical power. While as the shape becomes more ellipsoidal the cylindrical power increases. This is explained because a round cone's curvature is circularly symmetric around the cone's apex. Although, an oval cone's curvature and optical power is different in every direction away from the cone apex. The on axis cone's shape has little spherical equivalent power effect.

The cone's shape at the average location demonstrates a smaller cylindrical power dependence. The SE is affected by the cone's shape, because the oval cone's curvature is different for each radial direction. Thus in addition to the cone's shape the apex's horizontal and vertical distance from the visual axis will affect the optical power. The cone's shape at the far location has trivial optical power effects, because the curvature far from the cone's apex is nearly the same for different shapes.

The cone's shape has the most significant affect on higher-order aberrations. Oval cones located at the average position have the most high-order aberrations than any other cone configuration considered. At each location the rounder cones have less higher-order aberrations than the oval cones. This implies that round cones are corrected better

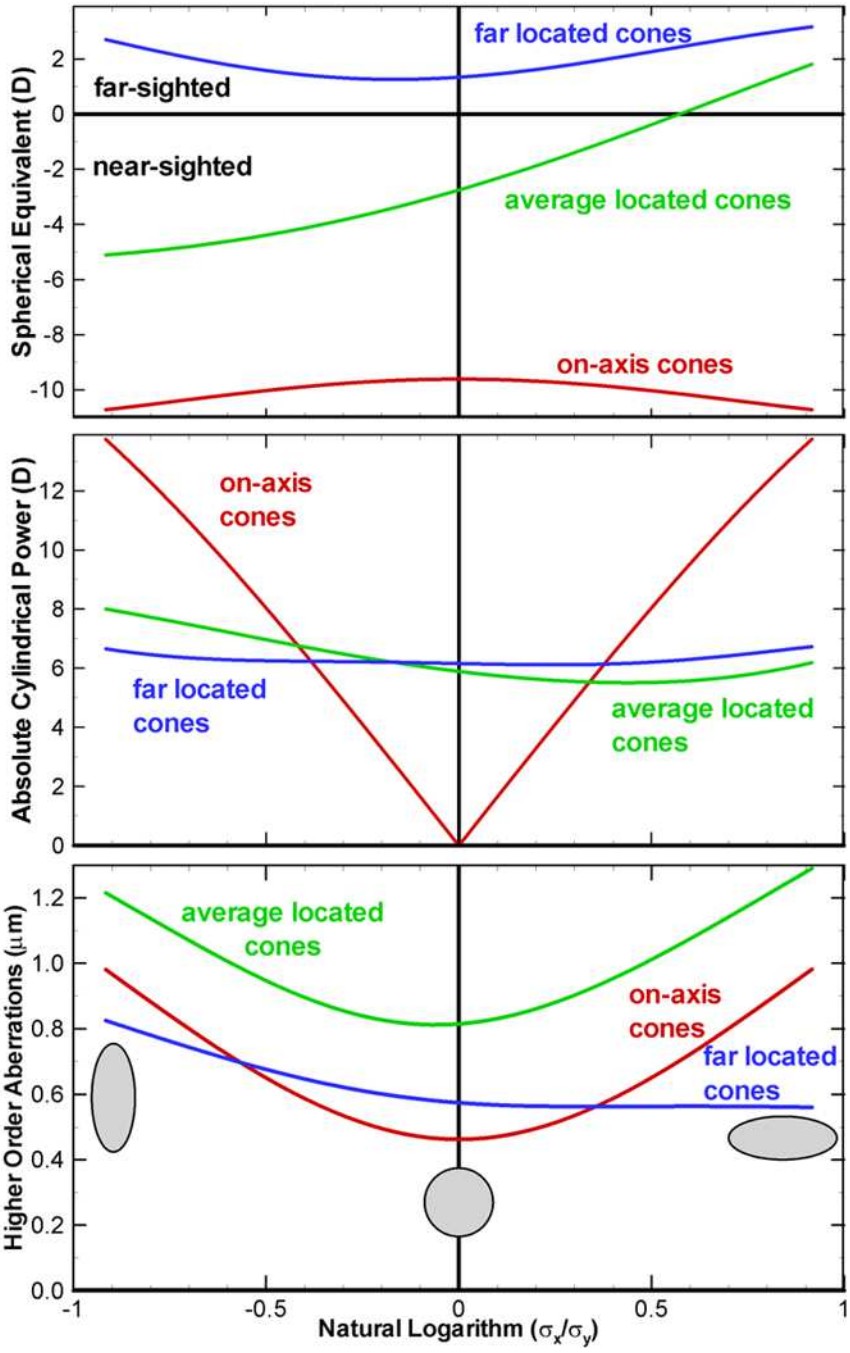

Figure 3.13: Keratoconus Cone Shape Visual Prescription Affects. Top: Spherical Equivalent Power. Middle: Absolute Cylindrical Power. Bottom: Root-mean-square of higher-order aberrations $W_{3,4}$.

with spectacles than oval cones.

Chapter 4

Keratoconus Analysis Using Photorefraction

Among the most valuable eye modeling applications is the ability to predict and evaluate conventional and new instrument detection capabilities. For KC detection the photokeratoscope is effective. However, it is a clinical-based device and not appropriate for large population screenings. Consequently, the majority of people have never been examined by such an instrument. In this chapter, the KC eye model is used to simulate a KC eye measurement result as observed with a device that is commonly used for vision screening. This instrument is based on photorefraction (PR) theory that will be discussed in the next section. The KC eye PR measurement result is compared with an astigmatic eye with the same refractive powers. Results are shown to illustrate how PR may be used to detect and differentially diagnose KC from normal astigmatic eyes.

4.1 Photorefraction Description

Photorefraction (PR) is a method to estimate the instantaneous refractive power by photographing the light refracted from a subject's eyes [10]. PR is based on the same principles as retinoscopy mentioned in section 1.2. The only difference is that an image is photographed. Chen performed PR theoretical analysis using three-dimensional ray tracing on realistic human eye models [11]. Therefore, a similar PR analysis is performed using the KC eye model.

There are two different PR image types: coaxial and eccentric images. As the name implies, coaxial PR occurs when the light source is aligned with the camera lens center. In eccentric PR, the light source is decentered near the camera's center. Each type has certain advantages and disadvantages. It is suggested that the simultaneous using both configurations, which is not currently done, will enhance the ability to diagnose KC.

In PR the light passes twice through the eye. The light rays reflected from normal, near-sighted, and far-sighted eyes are illustrated in Figure 4.1. This figure has the same configuration except the eye's optical power is different. The light rays reflecting from a normal eye retina exits parallel to the optical axis. However, a far (near)-sighted eye the light rays diverge (converge) from the eye. For such refractive eyes a crescent will appear in the pupil. An image taken of the pupil will appear dark for a normal eye, because no light rays enter the camera's aperture. Conversely, a near (far)-sighted eye has a bright crescent in the same (opposite) direction as the light source, Figure 4.1. If the camera and light source are interchanged the crescent rotates 180°.

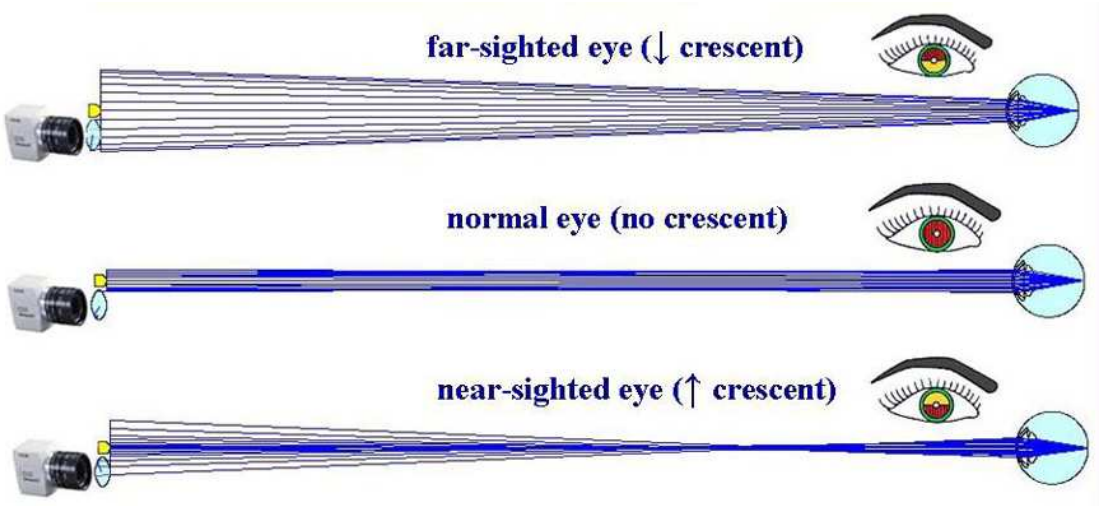

Figure 4.1: Eccentric Photorefraction For Farsighted, Normal, Nearsighted Eye.

To obtain the theoretical PR pupil image, the eye and the PR system parameters and are inserted into the optical software program. The parameters that are intrinsic to the PR calculation include: pupil diameter, camera aperture diameter, camera eccentricity, working distance, light source wavelength, shape and size of light source, and number of light rays to be calculated for each image. Table 4.1 identifies the PR parameters, gives the parameter values used in the calculation, and discusses the parameter's affect on the pupil's image. Since PR devices often acquire images in semi-darkened environments, the pupil diameter is set to 7 mm in these calculations. The camera's eccentricity, distance from optical axis, is either coaxial (on optical axis) or eccentric (15 mm decentered from optical axis) in the following PR calculations. Only a large camera eccentricity will capture light rays from sizable refractive eyes. This enables one to evaluate different refractive error degrees by varying the camera's eccentricity.

Table 4.1: Photorefraction Parameter Affects.

Parameter	Value used	Parameter's PR pupil image affect
Pupil Diameter	7 mm	When the pupil size is increased the refracted light becomes more spread out
Camera Aperture Diameter	20 mm	When aperture is increased more light rays enter the system, cone in pupil irradiance image becomes less distinct.
Camera Eccentricity	15 and 0 mm	Farther from the optical axis more severe KC degrees can be identified.
Working Distance	1 m	As the distance from the camera to the eye is increased the irradiance decreases
Number of Light Rays	100 million	The more light rays increases computation time, but cone in pupil irradiance image becomes more distinct.
Light Source Wavelength	555 nm	The eye reflects and absorbs wavelengths differently. The eye is most sensitive near this wavelength
Light Source Shape & Size	point source	The crescent for a line light source will be become more distinct.

4.2 Photorefraction Images of Keratoconus and Astigmatism of Same Equivalent Prescription

Using the photorefraction instrument it is advantageous to determine the observed pupil image differences between a KC and a normal refractive eye. To evaluate the differences, fifteen different KC eyes and the corresponding equivalent prescription refractive eyes are used to obtain theoretical PR irradiance pupil images. The fifteen KC eyes are modeled with five various cones at three different locations. The five various cones are chosen from the four volume regions mentioned in section 3.2, and also a round cone is included. The chosen cones are 2, 5, 7, 9, and 13 from table 3.1.

Figure 4.2 illustrates the coaxial PR irradiance pupil image for a centrally-, averagely-, and outlying- located KC cone. Each pupil image is scaled according to the maximum irradiance for that cone location. The left column corresponds to the KC cones located at the visual axis, middle column to average cone location, and right column to outlying cone location. The equivalent prescription results from section 3.2 is repeated below

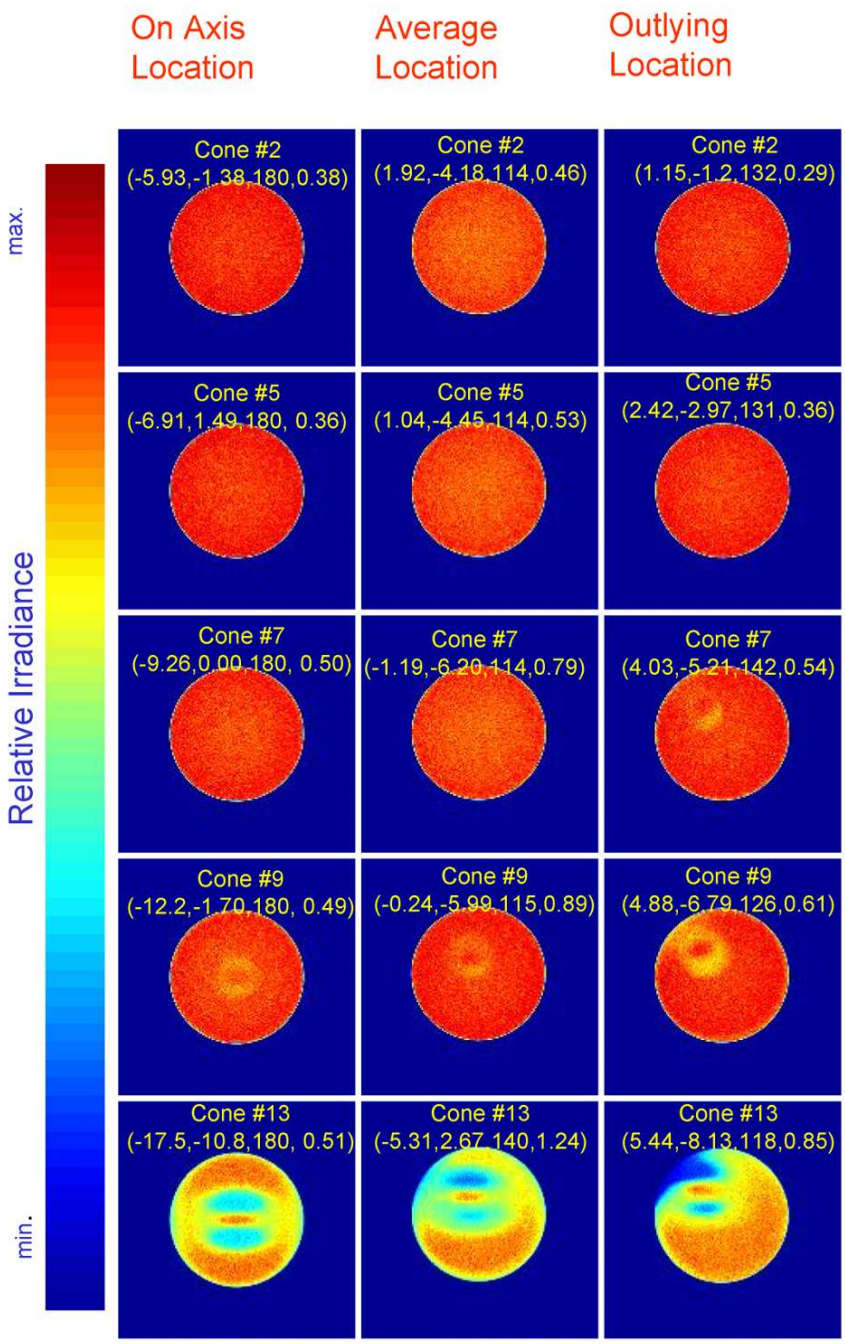

Figure 4.2: Keratoconus Coaxial Photorefraction Images In Three Different Locations. Left column corresponds to cones on visual axis, middle column to average cone location, and right column to outlying cone location. The four numbers correspond to Spherical (D), Cylindrical (D),Astigmatism Axis, $W_{3,4}$ (μm).

the cone number, in the form (spherical Diopters (D), cylindrical (D), astigmatism axis (degrees), $W_{3,4}$ (μm)).

To observe keratoconus using the coaxial PR technique the cone needs to be quite large. Cone # 9 presents the first detectable difference. The coaxial KC eye PR pupil image shows a decreased intensity (shadow) region. The decreased intensity region is believed to be the scissors reflex, or shadow that was seen in Figure 1.3. Therefore, mild KC cases cannot be detected using the coaxial PR method.

Eccentric PR irradiance pupil images for a centrally-, averagely-, and outlying- located KC cone are shown respectively in Figures 4.3, 4.4, and 4.5. Each pupil image is scaled according to the maximum intensity for that configuration, since the eye's reflectance is not known. The left column corresponds to the modeled KC eye's PR pupil image, while the right side corresponds to an astigmatic eye with the equivalent refractive prescription. The equivalent prescription is repeated again for direct comparison. The KC eye and the corresponding astigmatic eye have the same correctable prescriptions, while the high-order aberrations $W_{3,4}$ are different. Each astigmatic PR pupil image resembles the theoretical prediction obtained from Wesemann [28]. Wesemann evaluated eccentric PR images with mixed (irregular) astigmatism, two orthogonal spherical powers are near- and far- sighted, and determined that the crescent rotates along the rim of the pupil with increasing astigmatism axis.

One goal during this investigation is to determine if a PR vision screening instrument can detect and also differentiate KC from normal refractive errors. Each simulated KC

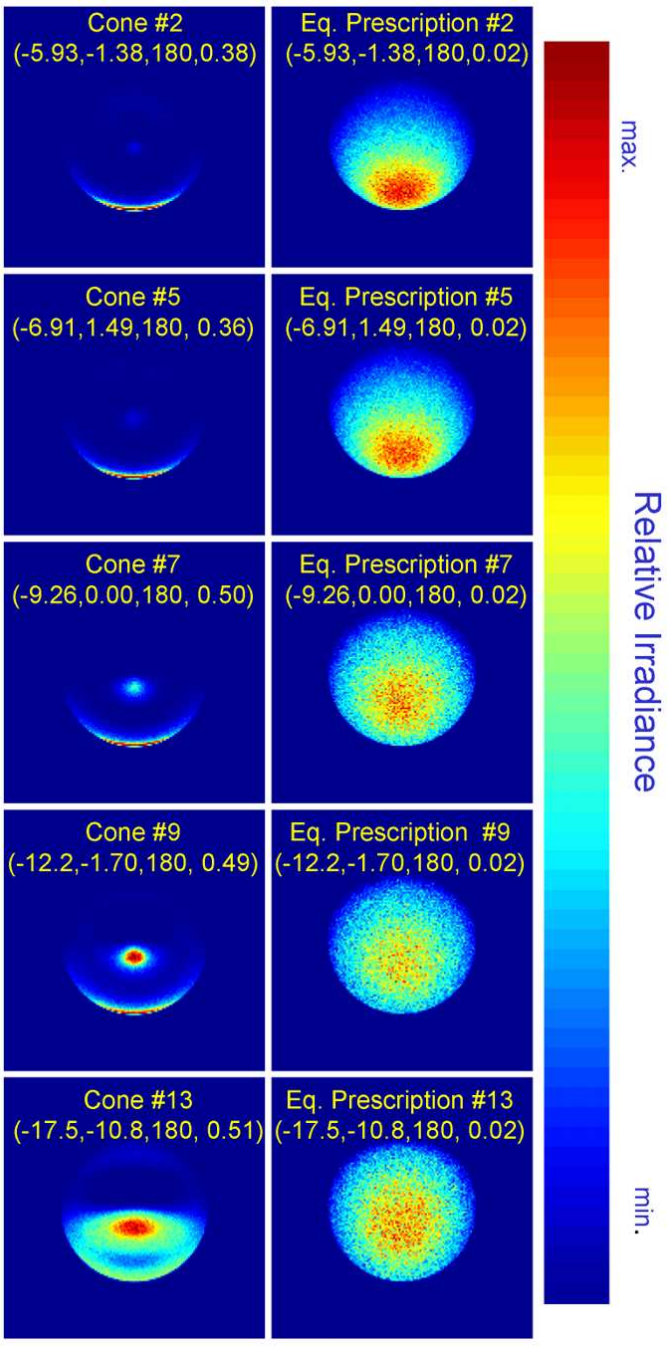

Figure 4.3: Keratoconus Eccentric Photorefraction Pupil Image For Cones Located On Visual Axis. Left column corresponds to KC eyes, while right column corresponds to Equivalent Astigmatic Eyes. The four numbers correspond to Spherical (D), Cylindrical (D), Astigmatism Axis, $W_{3,4}$ (μm).

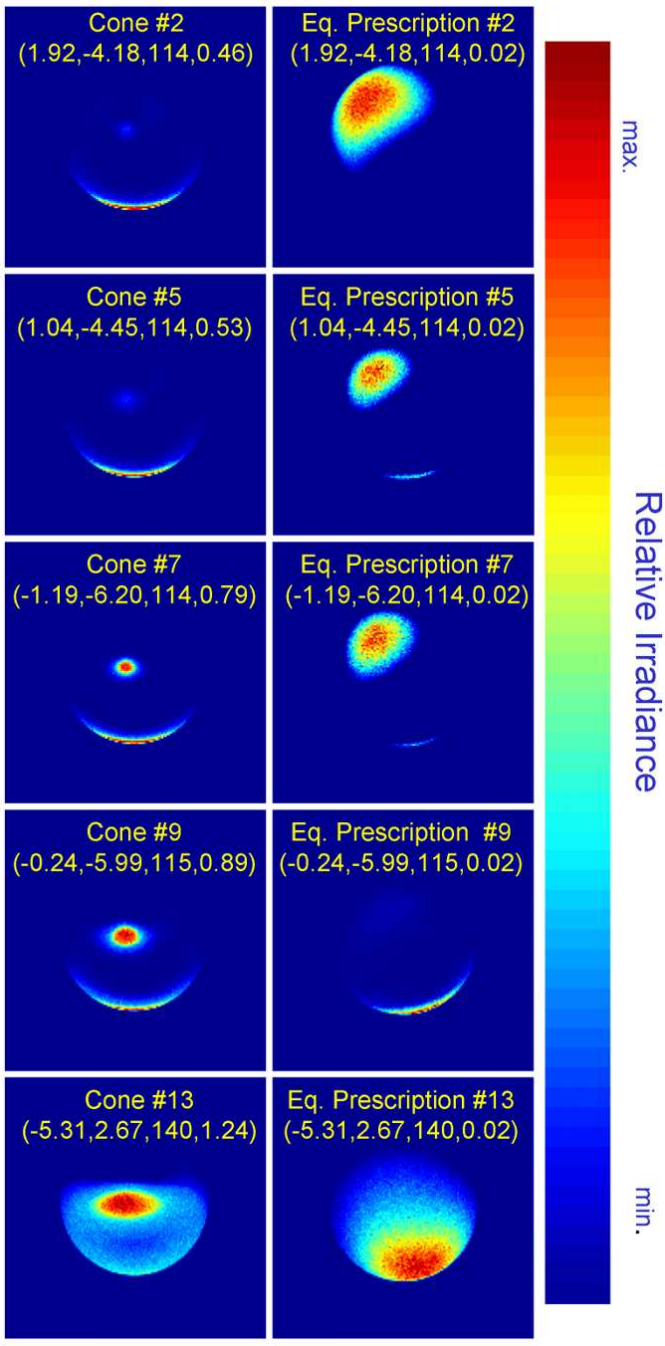

Figure 4.4: Keratoconus Eccentric Photorefraction Pupil Image For Cones Located At Average Position. Left column corresponds to KC eyes, while right column corresponds to Equivalent Astigmatic Eyes. The four numbers correspond to Spherical (D), Cylindrical (D), Astigmatism Axis, $W_{3,4}$ (μm).

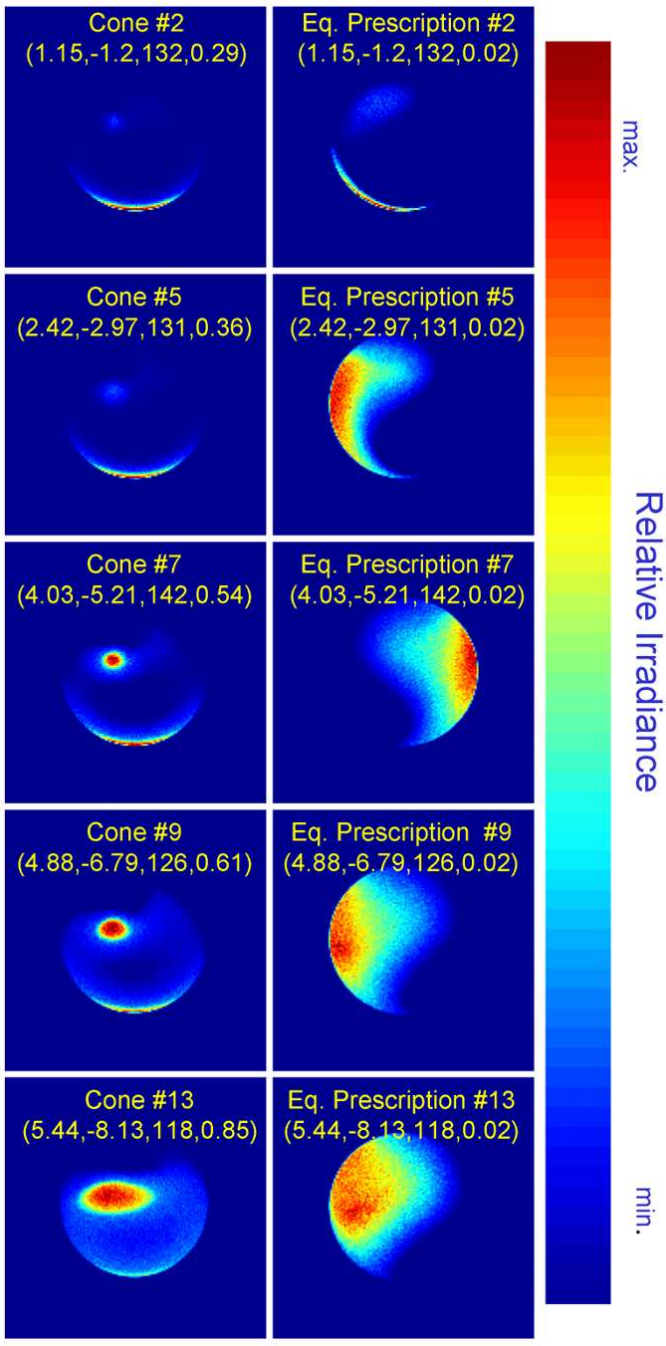

Figure 4.5: Keratoconus Eccentric Photorefraction Pupil Image For Cones Located At Outlying Position. Left column corresponds to KC eyes, while right column corresponds to Equivalent Astigmatic Eyes. The four numbers correspond to Spherical (D), Cylindrical (D), Astigmatism Axis, $W_{3,4}$ (μm).

eccentric PR pupil image indicates an irradiance region corresponding to the KC cone. Even the smallest KC cone #2 has a small irradiance region. This implies that the PR instrument is capable of detecting mild KC cases.

The PR irradiance pupil image also appears to differentiate KC from the equivalent correctable astigmatic eye. The PR irradiance crescent region lies on the pupil's periphery for each equivalent astigmatic eye. Conversely, each KC PR image has an isolated irradiance region located near the pupil's image interior. An astigmatic eye's PR irradiance image is typically less than a KC eye. This cannot be seen since each PR pupil image has its own irradiance scale.

The cone's size and location can also be described qualitatively from the KC PR pupil image. The cone height correlates with the irradiance. The cone volume corresponds to the flux through the PR image's irradiance region. Similarities in the cone's shape are also noticed in the PR pupil irradiance image, by comparing Figure 3.6, the cone's height map, and the corresponding KC PR image. A correlation between the cone's location and the PR image's irradiance region location is similarly observed. Also, the irradiance decreases when the cone is moved further from the visual axis.

The features of a KC PR pupil image show great potential for detecting and differentiating KC eyes. However, obtaining quantifiable KC cone characteristics using the PR technique requires further theoretical investigation. Also, clinical trials are required to validate the simulated PR results.

Chapter 5

Summary

Before this investigation little was known as to how a KC corneal cone's characteristics affect the eye's vision. Also, no known research has been done to identify a screening instrument to detect KC.

This thesis proposed and constructed an optical KC eye model for the first time. The visual performance was theoretically investigated for different KC degrees. Three independent cone characteristics were considered: dimension (volume), location, and shape. A photorefraction screening instrument was investigated as a possible new way to detect and differentially diagnose KC.

There are several conclusions obtained from this thesis:

1. A KC patient's visual performance is dominated by the effective cone curvature near the visual axis. i.e. ~ 3 mm-diameter range around corneal center.

2. KC cones on the visual axis procure a significant spherical refractive error (near-

sightedness). The cylindrical refractive error for on axis cones drastically depends on the cone's shape. However, the un-correctable high-order aberrations are smallest for the on axis KC cones. This implies that eye spectacles can correct on axis cones better than that of off axis cones.

3. KC cones on the visual axis procure a significant spherical refractive error (near-sightedness). The cylindrical refractive error for on axis cones drastically depends on the cone's shape. However, the un-correctable higher-order aberrations are smallest for the on axis KC cones. This implies that eye spectacles can correct KC cones located on the visual axis better than off the visual axis.

4. The PR technique, especially eccentric PR, can detect and distinguish refractive errors (near- and far-sighted and astigmatism) from KC easily. Clinical trials are required to validate simulated results.

Some future research plans may include:

1. Developing a more quantifiable KC classification system. The current ways to classify KC are very simple and rudimentary. A more rigorous classification system might include quantifiable cone parameters that describe the shape, location, and KC progression over time.

2. Modeling the internal corneal surface. Nearly $\frac{2}{3}$ of the eye's optical power occurs at the air/corneal surface interface. Therefore, the current KC eye model only modifies the outside corneal surface. The inner corneal surface is also different

from a normal eye. Therefore, in some calculations additionally modeling the inside corneal surface may represent a KC eye better than the current KC eye model.

3. Quantifying the KC cone structure and location from the PR pupil image. The KC cone structure and location were seen as qualitative characteristics from the KC PR theoretical pupil image. Analyzing more KC PR pupil images may obtain quantitative cone characteristics (height, shape, and location) from the PR irradiance pupil image.

Bibliography

Bibliography

[1] J.H.Krachmer, R. S. Feder, and M. W. Berlin. Keratoconus and Related Noninflammatory Corneal Thinning Disorders. *Surv. Opthalmol*, 28:293-322, 1984.

[2] N. Morlet, D. Minassian, and J. Dart. Astigmatism and the analysis of its surgical correction. *B. J. Opthalmol*, 85:1127-1138, 2001.

[3] D. Burger, J. P. Shovlin, and K. Zadnik. Center for Keratoconus. http://www.kcenter.org/disease_info/Keratoconus.html, 2003.

[4] H.D. Perry, J.N. Buxton, and B.S. Fine. Round and Oval Cones in Keratoconus. *American Academy of Opthalmology*, 87:905-909, 1980.

[5] P.G. Swann, H.E. Waldron. Keratoconus: The clinical spectrum. *Journal of the American Optometric Association*, 57:204-209, 1986.

[6] S.E. Wilson, D.T.C. Lin, and S.D. Klyce. Corneal Topography of Keratoconus. *Cornea*, 10:2-8, 1991.

[7] J. Schwiergerling, J. E. Greivenkamp, and J. M Miller. Representation of videokeratoscopic height data with Zernike polynomials. *J. Opt. Soc. Am. A*, 12:2105-2113, 1995.

[8] J. Y. Wang and D. E. Silva. Wave-front interpretation with Zernike polynomials. *Applied Optics*, 19:1510-1518, 1980.

[9] A. Prata Jr. and W. V. T. Rusch. Algorithm for computation of Zernike polynomials expansion coefficients. *Applied Optics*, 28:749-754, 1989.

[10] H. C. Howland, O. Braddick, J. Atkinson, and B. Howland. Optics of photorefraction: orthogonal and isotropic methods. *J. Opt. Soc Am.* 73:1701-1708, 1983.

[11] Y. L. Chen, B. Tan, and J. W. L. Lewis. Simulation of eccentric photorefraction images. *Optics Express*, 11:1628-1642, 2003

[12] W. R. Bobier and O. J. Braddick. Eccentric photorefraction: optical analysis and empirical measures. *Am. J. Optom. & Physiol Optics*, 62:614-620, 1985.

[13] W. R. Bobier, M. C. W. Campbell, C. R. McCreary, A. M. Power, and K. C. Yang. Coaxial photorefractive methods: an optical analysis. *Applied Optics*, 31:3601-3615, 1992.

[14] A. Gullstrand. The optical system of the eye. *Appendices to part 1. In: Von Helmholtz H. Physiological Optics.* 3^{rd} *ed. Vols 1 and 2.* 350-358, 1909.

[15] H. Von Helmholtz. *Phsiological Optics* 3^{rd} *ed. Vols 1 and 2.* 91-121, 1909.

[16] I. Escudero-Sanz and R. Navarro. Off-axis aberration of a wide-angle schematic eye model. *J. Opt. Soc. Am. A.*, 16:1881-1891, 1999.

[17] J. E. Greivenkamp, J. Schwiegerling, J. M. Miller, and M. D. Mellinger. Visual acuity modeling using optical raytracing of schematic eyes. *Am. J. Opthalmol.*, 120:227-240, 1995.

[18] H. Liou and N. Brenan. Anatomically accurate, finite model eye for optical modeling. *J. Opt. Soc. Am. A.*, 14:1684-1695, 1997.

[19] *Zemax User's Guide, Version 10.0.* Focus Software, Inc.

[20] T. T. McMahon, J. B. Robin, K. M. Scarpulla, and J. L. Putz. The spectrum of topography found in keratoconus. *CLAO journal*, 17:198-204, 1991.

[21] J. Schwiegerling and J. E. Greivenkamp. Keratoconus detection based on videokeratoscopic height data. *Optom. Vis. Sci.*, 73:721-728, 1996.

[22] J. Schwiegerling. Cone dimensions in keratoconus using zernike polynomials. *Optom. Vis. Sci.*, 74:963-969, 1997.

[23] A. Langenbucher, B. Seitz, M. M. Kus, and G. O. H. Naumann. Zernike representation of corneal topography height data after nonmechanical keratoplasty. *Invest. Opthalmol. Vis. Sci.*, 40:582-591, 1999.

[24] R. A. Applegate, R. Nuñez, J. Buettner, and H. C. Howland. How accurately can videokeratographic systems measure surface elevation? *Optom. Vis. Sci.*, 72:785-792, 1995.

[25] M. Born and E. Wolf. *Principles of Optics*. (Cambridge University Press 2002), Appendix VII.

[26] G. B. Arfken and H. J. Weber. *Mathematical Methods For Physicists*. (Harcort/Academic Press 2001), 596-601.

[27] R. G. Dorsch, W. A. Haimerl, and G. K. Esser. Accurate computation of mean power and astigmatism by means of Zernike polynominals. *J. Opt. Soc. Am. A.*, 15:1686-1688, 1998.

[28] W. Wesemann, A. M. Norcia, and D. Allen. Theory of eccentric photorefraction (photoretinocopy): astigmatic eyes. J. *Opt. Soc. Am. A.*, 8:2038-2047, 1991.

Vita

Kevin Charles Baker was born on November 18, 1979 in Mitchell South Dakota. He lived with his parents until the age of 18, when he moved in with his wife Jennifer. Kevin graduated from South Dakota School of Mines and Technology with a bachelor of science in physics and a minor in mathematics in May 2003. He is currently working towards his PH.D. in physics at the University of Tennessee Space Institute.